DEGREE PROJECT IN BIOTECHNOLOGY,
SECOND CYCLE, 30 CREDITS
STOCKHOLM, SWEDEN 2021

Subcellular mapping of cell types in healthy human pancreatic islets

FRIDA BJÖRKLUND

KTH ROYAL INSTITUTE OF TECHNOLOGY
SCHOOL OF ENGINEERING SCIENCES IN CHEMISTRY, BIOTECHNOLOGY AND HEALTH

Subcellular mapping of cell types in healthy human pancreatic islets

Frida Björklund
Supervisor: Dr. Emma Lundberg
Co-supervisor: Dr. Anna Martinez Casals
Examiner: Dr. Patrik Ståhl

2021-05-31

ABSTRACT

Pancreatic islets are composed of endocrine cells that secrete hormones essential for blood-glucose homeostasis. Prior research has revealed that the gene expression and functionality of human islet cells is heterogenous. However, it is not currently understood how the heterogeneity correlates to normal islet cell function and dysfunction in diabetes pathogenesis. Subsequently, an international collaborative project has been initiated to elucidate what constitutes islet cell heterogeneity from a transcriptional, proteomic, and functional perspective in both health and disease. In this study, a highly multiplex tissue image assay was developed to allow for the study of the localization and distribution of proteins previously identified to correlate with functional activity and heterogeneity in islet cells using the CO-Detection by indEXing (CODEX) platform. In total, 22 proteins were studied simultaneously of which 10 were specifically expressed in islet cells. These included generic pancreatic markers such as C-peptide (C-pep) marking insulin-secreting β-cells, glucagon (GCG) and somatostatin (SST), but also less well-characterized proteins such as Shisa like 2B (FAM159B) and Neural proliferation, differentiation and control 1 (NPDC1). The multiplex tissue imaging allowed for single-cell analysis of protein expression in human islet cells showing that most islet specific proteins were heterogeneously expressed. The observations made in this study serves as a validation to that the human islet microenvironment is highly complex due to islet cell heterogeneity. Additionally, the study demonstrated that multiplex tissue imaging has the potential to reveal novel cell types and interactions.

SAMMANFATTNING

Langerhanska öar består av endokrina celler som utsöndrar hormoner nödvändiga för reglering av blodsockernivåerna. Tidigare forskning har visat att genuttrycket och funktionaliteten är heterogen i de celler som utgör mänskliga Langerhanska öar. Dock är förståelsen för hur heterogeniteten korrelerar till normal cellfunktion och dysfunktion i diabetespatogenes fortfarande ofullständig. Följaktligen har ett internationellt samarbete inletts i syfte att undersöka vad som utgör heterogenitet i Langerhanska öar ur ett transkriptionellt, proteomiskt och funktionellt perspektiv i såväl friska som sjuka individer. I denna studie utvecklades en metod för multiplex mikroskopisk avbildning av vävnad för att möjliggöra undersökningen av hur proteiner som tidigare korrelerats med endokrin cellspecifik aktivitet och heterogenitet i Langerhanska öar var lokaliserade med hjälp av plattformen för Co-Detection by indEXing (CODEX). Totalt undersöktes 22 proteiner samtidigt varav 10 var specifikt uttryckta i celler som utgör Langerhanska öar. Bland dessa proteiner fanns generella markörer för vanligt förekommande celltyper i Langerhanska öar såsom C-peptid (C-pep) som markör för insulinsekreterande β-celler, glukagon (GCG) och somatostatin (SST) såväl som proteiner med färre kända funktioner såsom Shisa like B (FAM159B) och Neural proliferation, differentiation and control 1 (NPDC1). Med hjälp av multiplex mikroskopisk avbildning av vävnad kunde uttrycket av proteiner specifikt uttryckta i celler som utgör Langerhanska öar analyseras för enskilda celler i vävnaden. Denna analys visade att de flesta proteiner specifikt uttryckta i celler som Langerhanska öar består av var heterogent uttrycka. Resultaten från denna studie validerar att mikromiljön i Langerhanska öar är mycket komplex på grund av cellernas heterogenitet. Vidare visade denna studie att multiplex mikroskopisk avbildning av vävnad har potentialen att identifiera nya celltyper och interaktioner.

Keywords
Pancreatic islets · Immunostaining · Multiplex tissue imaging · CODEX · DNA-conjugated antibodies · Spatial cell biology · Proteomic profiling

TABLE OF CONTENTS

INTRODUCTION

The pancreas is a bifunctional, glandular organ composed of two different compartments, namely the exocrine and endocrine compartment [1]. The exocrine compartment is predominantly composed of enzyme-secreting cells. The metabolic enzymes are secreted to the gastrointestinal tract and are essential for digestion of ingested food. The endocrine compartment is composed of disparate collections of endocrine pancreatic cells. The collections of endocrine pancreatic cells are referred to as pancreatic islets, or Islets of Langerhans, and secrete hormones that uphold blood-glucose homeostasis [2, 3]. Pancreatic islets are composed of at least four cell types: β-, α-, δ-, and pancreatic polypeptide (PP)-cells. β-cells produce and secrete insulin (INS) in response to increased blood-glucose levels which stimulates peripheral cells to increase their glucose uptake. α-cells produce and secrete glucagon (GCG) in response to decreased levels of glucose in the blood and promotes peripheral cells to release glucose to the blood. δ-cells produce and secrete somatostatin (SST) which acts as a balancing hormone by regulating the effect of insulin and glucagon to ensure that blood-glucose homeostasis is maintained. PP-cells contain pancreatic polypeptide which acts as an inhibitor to glucagon, and they have also been shown to have an important role in facilitating intra-islet communication [3].

Studies of human pancreatic islets have demonstrated that human islets display unique structural and functional characteristics [4, 5]. The cytoarchitecture of human islets is not yet entirely understood since it in some instances has been observed that islets have a seemingly clear organization where α-cells are segregated from other islet cell types, localized to the islet mantle, while it in other instances have been observed that islet cells are stochastically dispersed throughout the islet with no apparent internal organization [5, 6]. Moreover, human islet cells have been shown to favour heterotypic interactions over homotypic interactions within the islets, suggesting that the paracrine signalling network regulating glucose homeostasis is highly complex [4, 7]. Additionally, studies have demonstrated that islet cells display heterogeneity in both gene expression and functionality, existing as different subpopulations within the islets, which adds to the complexity of the human islet microenvironment [8-12]. However, it is not yet fully understood how islet cell heterogeneity correlates to cell function in health and disease. Consequently, efforts are being made to elucidate what constitutes islet cell heterogeneity.

One such effort is the international collaborative project Human Islet Research Network (HIRN), funded by the National Institute of Health (NIH). The collaborative project aims to investigate islet cell transcriptional, proteomic, and functional heterogeneity in health and in type 1 diabetes by making use of recent technological advancements that have enabled detailed studies of transcriptional and proteomic variability at the single-cell level [8]. As part of the collaborative project, transcriptomes of 1,369 human islet cells were investigated by combining electrophysiological measurements of exocytosis and channel activity with single-cell RNA sequencing (scRNA-seq), i.e. patch-seq. Exocytosis is the process in which cells transport molecules from within to the extracellular space and is a fundamental function of hormone secreting cells. This analysis resulted in the detection of a subset of heterogeneously expressed genes that correlated with the functional activity and heterogeneity of human islet cells [12]. The subset of genes will be investigated as proteomic markers, using a multiplex antibody-based approach, to study islet cell phenotypes and their interactions in a preserved histological context.

Protein function is intimately connected with subcellular localization since cellular compartments provide specialized environments in which only certain reactions and interactions can occur. It is therefore essential to study the localization and dynamics of proteins at the subcellular level to attain a deepened understanding of cell biology [13-15]. Additionally, it is important to study cellular localization and cellular interactions to understand the underlying mechanisms of tissue homeostasis and disease characteristics. Presently, identification of cells and cell phenotypes through proteomic profiling is primarily done with immunohistochemistry and immunofluorescence imaging. These technologies are, however, limited to the number of proteins that can be studied simultaneously. Yet, it has been demonstrated that to accurately identify phenotypes and cell populations within a tissue sample, multiple proteins need to be analysed at the same time [8, 16]. Consequently, there have been several recent technological developments in multiplex tissue imaging, allowing numerous protein targets to be analysed within one tissue sample [17]

One example of a multiplex tissue imaging technology is the CO-Detection by indEXing (CODEX) system [16]. In the CODEX technology, a tissue sample is first stained with DNA-barcode conjugated antibodies. Second, a maximum of three fluorescently labelled DNA reporter oligonucleotides complementary to the DNA-barcode conjugated antibodies are added to onto the tissue sample. Third, the fluorescently labelled DNA reporters that have hybridized to the corresponding DNA-barcode conjugated antibodies are imaged using fluorescence microscopy. Fourth, the reporter oligonucleotides are removed, and the tissue is washed to allow for the process to be repeated. This iterative process of annealing, imaging, and stripping is performed by an automated fluidics system and is repeated to capture the spatial information of up to 40 proteins simultaneously [16-19].

Aim

The primary aim of the project was to build an assay to visualize, annotate, and analyse cell types in healthy human pancreatic islets using the CODEX platform to aid in the generation of a spatially resolved map of the islet microenvironment. By studying the spatial localization and distribution of proteins in islet cells, the understanding of islet cell biology and the islet microenvironment can be improved in both health and disease. Another aim of the project was to expand the library of in-house DNA-barcode conjugated antibodies to aid in the development of a novel multiplex antibody panel targeting proteins specifically expressed in human pancreatic islets for future research projects.

MATERIALS AND METHODS

All human pancreas tissue samples used in this project came from diseased non-diabetic donors and were provided by the Alberta Diabetes Institute (ADI) IsletCore (Canada), according to board-approved ethical permits (DNR: 2020-01690). The ADI have established a distribution programme in collaboration with procurement organizations who make certain that each organ is ethically sourced, and that the donor information is safeguarded.

Antibody screening by indirect immunofluorescence

Commercially available antibodies toward protein targets identified to be heterogeneously expressed in islet cells by the collaborative project were selected and screened using indirect immunofluorescence to ensure target specificity prior to conjugation. Additionally, all screened antibodies were free from carrier proteins, *e.g.* BSA, stored in saline solutions such as PBS, had low concentrations of preservatives, *e.g.* sodium azide, had high concentrations (0.1-1mg/mL) of antibody and had been validated to function in immunohistochemical assays with formalin-fixed paraffin embedded (FFPE) tissue sections using heat-induced epitope retrieval (HIER) at pH 6 (Appendix 1). These abovementioned criteria for antibody selection were critical to assure that no reagents would interfere with the DNA-barcode antibody conjugation and that all antibodies would be functional in the same conditions.

To screen the antibodies, FFPE pancreas tissue sections from healthy human donors known to express the targeted proteins were used as a positive control. First, the FFPE tissue sections were baked at 55°C for 25min and, subsequently, allowed cooled down for 5min. Second, the tissue sections were deparaffinized and rehydrated in (1) HistoChoice Clearing Agent (2x5min), (2) 100% ethanol (2x5min), (3) 90% ethanol (1x5min), (4) 70% ethanol (1x5min), (5) 50% ethanol (1x5min), (6) 30% ethanol (1x5min), and (7) MilliQ H_2O (2x5min) at RT. For antigen retrieval, the tissue samples were submerged in citric acid (1:100 in MilliQ H_2O, pH6) and placed in a pressure cooker (high pressure, 114-121°C, 20min) and, subsequently, left to cool down in the solution for approximately 15min before they were transferred to MilliQ H_2O (2x2min). To reduce autofluorescence from the acinar tissue, the samples were photobleached (4.5% H_2O_2, 20nM NaOH in 1X PBS) through incubation between two LED-lights at maximum capacity (1x45min) and thereafter washed with 1X PBS (4x3min). Next, the samples were incubated with the primary antibody (diluted in 0.3% Triton in 1X PBS) in a humidity chamber at 4°C overnight (Appendix 1). Following the overnight incubation, the samples were washed with 1X TBS 0.1% Tween (3x15min). Next the samples were incubated with fluorescently labelled secondary antibodies (1:800 antibody and 1:800 Hoechst nuclear stain in TNB buffer (0.5% TSA blocking buffer in 1X TBS)) in a humidity chamber (90min, RT) before washed with 1X TBS 0.1% Tween (3x15min). Finally, coverslips were mounted onto the samples with Fluoromount-G mounting media, sealed with nail polish, and left to dry before image acquisition.

Antibody DNA-barcode conjugation

The commercial antibodies that had shown target specificity and high signal to noise ratios (SNR) were subsequently conjugated with unique oligonucleotide barcodes. The SNR was calculated using the equation presented in Appendix 2. According to the manufacturer of the CODEX system, the SNR of the screened antibody needed to exceed 3 to allow for clear distinction between the signal from antibody staining signal and noise present in the image. Therefore, SNR > 3 was used as a selection criteria for the screened antibodies. Besides the commercial antibodies that had been screened during the project, three additional commercial antibodies screened prior to the beginning of the master thesis project were also conjugated. Moreover, four antibodies internally developed in the Human Protein Atlas (HPA) project were especially purified to meet the abovementioned criteria for antibodies to be compatible with the CODEX system [20]. The HPA antibodies were conjugated without prior screening as they were known to display target specificity in preceding rigorous antibody validation (Appendix 3).

CODEX® Filter Blocking Solution was added on top of 50kDa MWCO filters, one for each antibody to be conjugated, centrifuged down (12,000g, 2min) and the residual liquid was removed from the columns. The volume corresponding to 50µg of antibody was thereafter added onto the columns and spun down (12,000g, 8min). The flow-through was removed and CODEX® Antibody Reduction Master Mix was added to the columns, incubated for 30min at RT and subsequently spun down (12,000g, 8min). Next, the flow-through was removed and the columns were equilibrated with CODEX® Conjugation Solution (12,000g, 8min) before the resuspended lyophilized DNA-barcodes (Nuclease-free water and CODEX® Conjugation Solution) were added onto each column and incubated for 2h at RT. Following the 2h incubation, the columns were centrifuged (12,000g, 8min) and the flow-through was removed before CODEX® Purification Solution was added onto each column which, subsequently, was spun down (12,000g, 8min). The conjugated antibodies were purified for a total of three times by the repeated addition of CODEX® Purification Solution, centrifugation (12,000g, 8min) and removal of residual liquid in the column. After the third wash, CODEX® Antibody Storage Solution was added onto each column that, subsequently, was inverted into a new tube before centrifugation (3,000g, 2min) to collect the purified, conjugated antibody. The conjugated antibodies were then stored at 4°C.

Validation of conjugated antibodies via tissue staining

To ensure that the antibodies had been successfully conjugated and had retained their target specificity, the DNA-barcode conjugated antibodies were validated through immunofluorescence by staining FFPE pancreas tissue sections and manual addition of fluorescently labelled DNA reporter oligonucleotides. Before the conjugated antibodies were used for tissue staining, they had been stored at 4°C for a minimum of 48h to avoid high levels of background nuclear staining. The same protocol for baking, deparaffinization, rehydration, antigen retrieval and photobleaching was used to stain the FFPE pancreas tissue sections for the validation of the conjugated antibodies as for the antibody screening. Following the washes with 1XPBS (4x3min) the tissue was washed with CODEX® Hydration Buffer (3x30s) and incubated with CODEX® Staining Buffer in a hydration chamber for 20min at RT. Next, the tissue was incubated with the conjugated antibody diluted in CODEX® Blocking Buffer in a humidity chamber at 4°C overnight. Each conjugated antibody was validated in two dilutions, 1:50 and 1:100, to determine which dilution resulted in the highest SNR. After the overnight incubation, the tissue samples were washed with CODEX® Staining Buffer (3x30s), incubated for 2min at RT, and washed with CODEX® Staining Buffer for an additional 3x30s. Next, the samples were incubated with a 1.6% solution of PFA (16% PFA diluted in CODEX® Storage Buffer) for 10min at RT for post-fixation of the tissue sections. The tissue sections were thereafter washed with 1X DPBS (3x30s) prior to 5min incubation with ice-cold 100% methanol. Following the ice-cold methanol incubation, the tissue sections were washed with 1X DPBS (3x30s) and incubated with CODEX® Fixative Solution (1:50 dilution of CODEX® Fixative Reagent in 1X DPBS) for 20min at RT in a humidity chamber. The tissue sections were thereafter washed with 1X DPBS (3x30s) prior to equilibration with CODEX® Screening Buffer (1:10 10X CODEX® Buffer and 1:5 DMSO in Nuclease-free water). Next, the fluorescently labelled DNA reporter oligonucleotides, diluted in CODEX® Reporter Stock Solution (1:20 CODEX® Assay Reagent and 1:400 Hoechst nuclear stain in CODEX® Screening Buffer), were added manually onto the tissue sections (1:40 dilution) and incubated for 5min at RT in a humidity chamber. Following the incubation with the fluorescently labelled DNA reporter oligonucleotides, the tissue sections were washed with CODEX® Screening Buffer (3x30s) and equilibrated with 1X CODEX® Buffer (1:10 10X CODEX® Buffer in MilliQ H_2O).

Next, coverslips were mounted onto the section with Fluoromount-G mounting media, sealed with nail-polish, and left to dry before image acquisition.

Multiplex tissue staining and imaging

Ensuing the validation of the DNA-barcode conjugated antibodies, two antibody panels for the multiplex tissue imaging were constructed – one for the imaging of a pancreas tissue section sample and one for the imaging of an isolated pancreatic islets sample (Appendix 4). To stain the tissue samples, the same protocol for baking, deparaffinization, rehydration and antigen retrieval was used. Photobleaching was only performed on the pancreas tissue section and not on the sample with isolated islets to ensure tissue integrity. Following the washes with 1X PBS, the samples were washed with CODEX® Hydration Buffer (2x10s) before they were equilibrated with CODEX® Staining Buffer for 30min at room temperature. The respective 22-plex antibody panel cocktail (diluted in CODEX® Blocking Buffer) was added onto each sample and incubated in a humidity chamber at 4°C overnight. After the overnight incubation, the same protocol for post-staining was used as for the validation of conjugated antibodies. Following the incubation with CODEX® Fixative Solution and washes with 1X DPBS, the tissue sections were placed in CODEX® Storage Buffer and stored at 4°C. Next, reporter cycle plates were constructed by the addition of the fluorescently labelled DNA reporters (diluted in CODEX® Reporter Stock Solution (1:10 10X CODEX® Buffer, 1:12 CODEX® Assay Reagent and 1:300 Hoechst nuclear stain in Nuclease free water)) in the order of the CODEX cycle arrangement. The diluted DNA reporters were transferred to the corresponding well in a 96-well plate. Additionally, two blanks containing only CODEX® Reporter Stock Solution was added to the 96-well plate which, subsequently, was sealed and stored at 4°C (Appendix 5).

To initiate the multiplex tissue imaging, the sample and the corresponding prepared reporter plate was equilibrated to RT. Experiment details was saved as a template in the CODEX® Instrument Manager (CIM, v. 1.29.3.6) (Appendix 5). The sample was placed in the microscope stage insert and the reporter plate was placed in the CODEX instrument. The sample was stained with nuclear stain (1:10 10X CODEX® Buffer and 1:160 Hoechst nuclear stain in MilliQ H_2O, 3min) and subsequently washed. Next, the microscope was set up for image acquisition by (1) finding the focus of the tissue, (2) selection the region of interest, (3) focusing the region of interest, and (4) setting the number of Z-stacks to be imaged. Lastly, the experiment was started in CIM.

Image acquisition, processing, and analysis

All images in the project were acquired at room temperature using Leica DMI8 widefield microscope at 20X magnification and 16-bit acquisition through the Leica Application Suite X (LAS X). The exposure times and focus of images acquired from antibody screenings and validations were set manually to acquire images with a high SNR (SNR >3, Appendix 2). The acquired images were visually inspected, merged, and analysed using ImageJ. The staining pattern of each antibody was compared to reference images provided by the manufacturer when available and the HPA Tissue Atlas to validate the observed staining pattern.

In the images acquired from the CODEX runs, the exposure times for each marker was pre-set in CIM and, subsequently, read into the LAS X throughout the imaging cycles (Appendix 5). The focus was set with the help of a focus map, where individual focus points were set in every other tile where tissue was present, and the focus of each point was found by autofocus. To correct for eventual irregularities, such illumination inhomogeneities, caused by the microscope's optics the "*Linked Shading*" feature was used.

Image processing was performed using the CODEX® Processor (v. 1.7.0.6) to prepare the images for downstream data analysis. In short, the image processing completes five actions that allows for data analysis at single-cell level. First, it aligns all images acquired for every individual tile that has been imaged. Secondly, it aligns the tiles and stitches the tiles together to create an image of the entire region of interest across all cycles. Thirdly, it subtracts background intensity signals caused by autofluorescence based on the blank cycles. Fourthly, it segments the cells within the image, i.e., it identifies and outlines the boundaries of each individual cell within the imaged tissue. Lastly, it measures the signal intensity of each marker within the boundaries of each segmented cell and provides additional data (cell ID, cell position) for downstream analysis. The processed images were thereafter visualized, annotated, and analysed in the CODEX® Multiplex Analysis Viewer (MAV, v. 1.5.0.8), an ImageJ plugin.

RESULTS

Antibody screening through indirect immunofluorescence

Of the 10 commercial antibodies toward islet specific markers that were screened in this study, only 2 displayed a specific staining pattern with a sufficiently high SNR (>3) to be conjugated with DNA-barcodes (Fig. 1A&B). The anti-MafA antibody (ab264418) could be observed to display a nuclear staining pattern specific to the islets and had a SNR of 9.8. The anti-RBP4 antibody (ab226137) was observed to have cytoplasmic staining pattern specific to cells localized in the pancreatic islets and a SNR of 11.0.

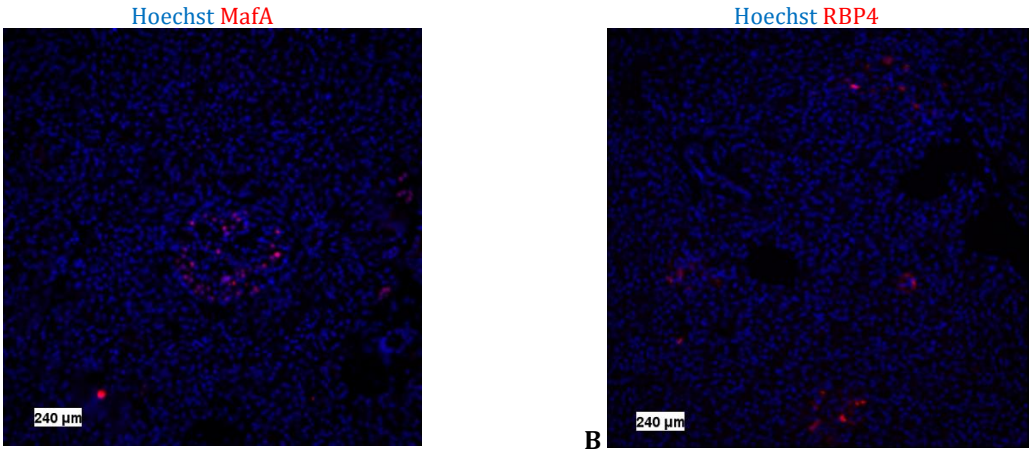

Figure 1. Antibodies screened through indirect immunofluorescence in human pancreas tissue sections where nuclei are visualised in blue (Hoechst) and the protein target in red. (A) Anti-MafA antibody (ab264418) diluted 1:100. Image acquisition: 20X, Cy5, 300ms. (B) Anti-RBP4 antibody (ab226137) diluted 1:100. Image acquisition: 20X, Cy7, 300ms.

Antibody validation of DNA-barcode conjugated antibodies

In total, 9 antibodies toward pancreatic markers were conjugated with unique DNA-barcodes. 8 of 9 antibodies were successfully conjugated where a specific staining pattern could be observed through direct immunofluorescence (Fig. 2A-I). One antibody (anti-ARX, MABN102) was not successfully conjugated with its unique DNA-barcode as no staining was detected (Fig. 2A). The conjugated antibodies towards C-peptide (C-pep) a marker for insulin-secreting β-cells, IAPP, ILF3, KRT19 and NPDC1 displayed a specific staining pattern and high SNR (40.2, 13.5, 11.9, 22.5 and 7.9, respectively) and were therefore included in the multiplex antibody panel. The antibodies targeting FAM159B and MafA had low signal intensities and SNR (2.9 and 2.4, respectively). However, they displayed a specific staining pattern, and were therefore included in the antibody panel at an increased concentration in an attempt to enhance the intensity of the signal (Appendix 4). A specific staining pattern for the conjugated antibody targeting RBP4 could be observed in the islets. Yet, there was a visible high background from the acinar tissue, resulting in a low SNR (2.5). Nevertheless, this antibody was included in the antibody panel since the high background signal potentially could be corrected through background subtraction in the image processing.

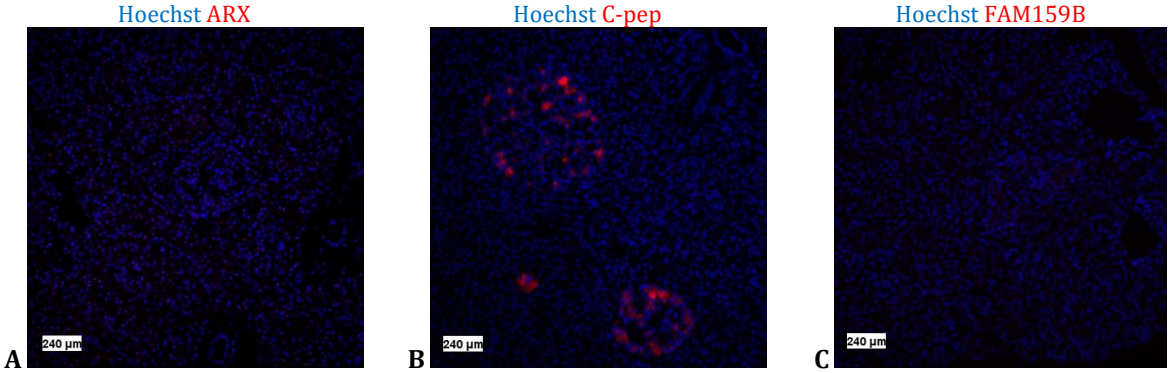

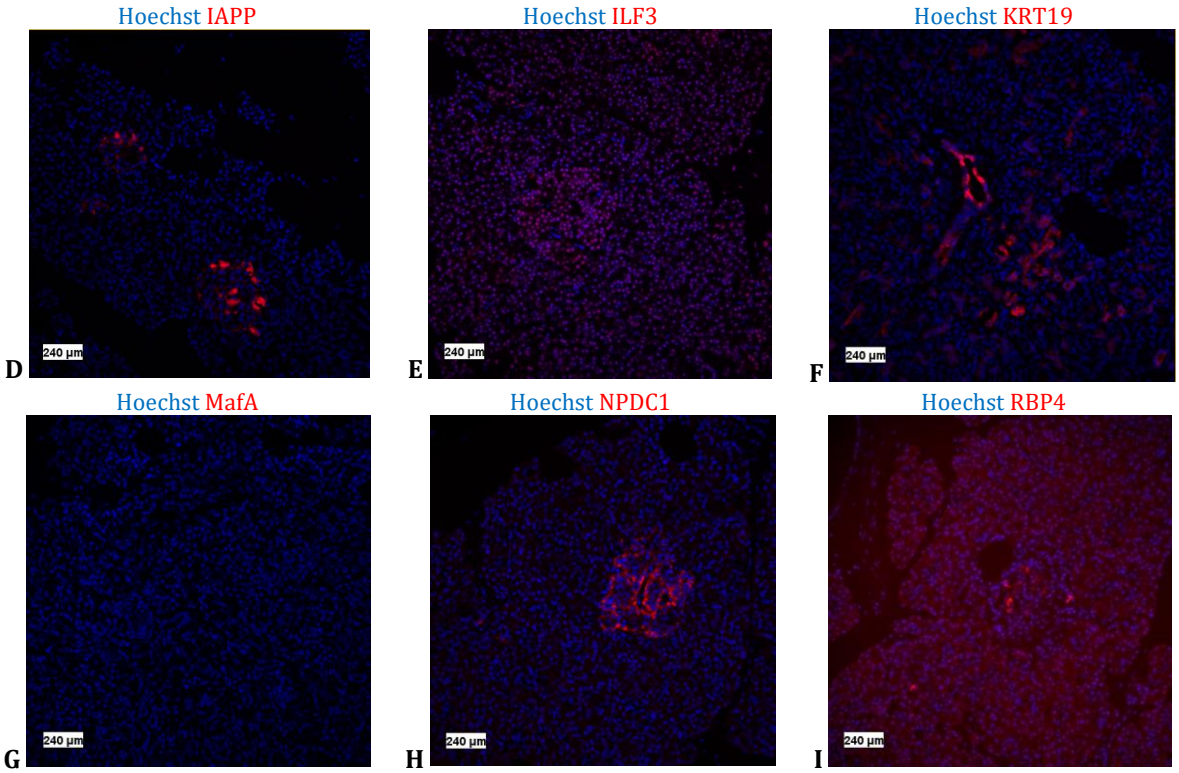

Figure 2. Validation of DNA-barcode conjugated antibodies by manual addition of fluorescently labelled DNA-reporters in human pancreas tissue sections where the nuclei are visualized in blue (Hoechst) and the protein target is visualized in red. (A) Conjugated anti-ARX antibody (MABN102) diluted 1:50. Image acquisition: 20X, Cy5, 700ms. (B) Conjugated anti-C-peptide antibody (MA1-19159) diluted 1:100. Image acquisition: 20X, Atto550, 100ms. (C) Conjugated anti-FAM159B (HPA011778) diluted 1:50. Image acquisition: 20X, Cy5, 700ms. (D) Conjugated anti-IAPP antibody (HPA053194) diluted 1:100. Image acquisition: 20X, Atto550, 300ms. (E) Conjugated anti-ILF3 antibody (HPA001897) diluted 1:100. Image acquisition: 20X, Atto550, 350ms. (F) Conjugated anti-KRT19 antibody (ab7754) diluted 1:100. Image acquisition: 20X, Atto550, 250ms. (G) Conjugated anti-MafA antibody (ab264418) diluted 1:50. Image acquisition: 20X, Cy5, 600ms. (H) Conjugated anti-NPDC1 antibody (HPA008189) diluted 1:100. Image acquisition: 20X, Cy5, 700ms. (I) Conjugated anti-RBP4 antibody (ab226137) diluted 1:50. Image acquisition: 20X, Cy7, 600ms.

Multiplex tissue imaging of isolated pancreatic islets

To image the isolated pancreatic islets a 22-plex panel of in-house DNA-barcode conjugated antibodies was used. 8 antibodies targeted proteins known to be specifically expressed in organelles of human cells, 1 targeted neurons, 12 targeted proteins specifically expressed in the pancreas and 1 was a mesenchymal marker (GRHL2) observed to be expressed in pancreatic islets in the HPA Tissue Atlas (Appendix 4). The entire region that was imaged is presented in Figure 3 and consisted of 3,127 cells. In Figure 3, two islets have been marked by a white rectangle to show which islets each marker has been visualized in (Fig. 4A-V).

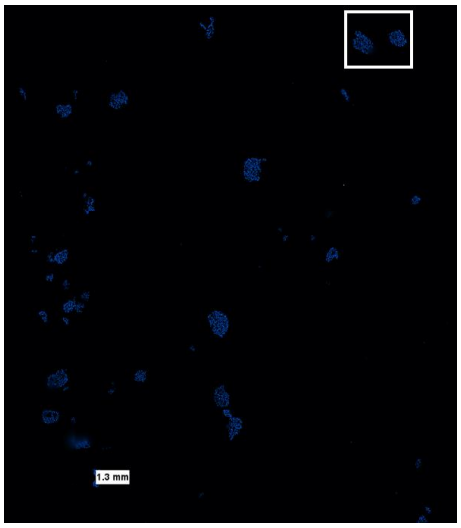

Figure 3. Sample overview of the isolated pancreatic islets where the nuclei are visualised in blue (Hoechst).

In Figure 4A-V, each of the 22 proteins targeted by the in-house conjugated multiplex antibody panel have been visualized individually. From the images it can be observed that there is no staining of either AMY2A or KRT19 within the tissue structures marked by the white rectangle in Figure 3, validating that the cells are islet cells as AMY2A only is expressed in exocrine pancreatic cells and KRT19 only is expressed in ductal cells. Moreover, it visible that the organelle markers are homogeneously expressed in all cells. Furthermore, there is a discernible difference in signal intensity in the pancreatic markers, indicating that the proteins are heterogeneously expressed in the islet cells.

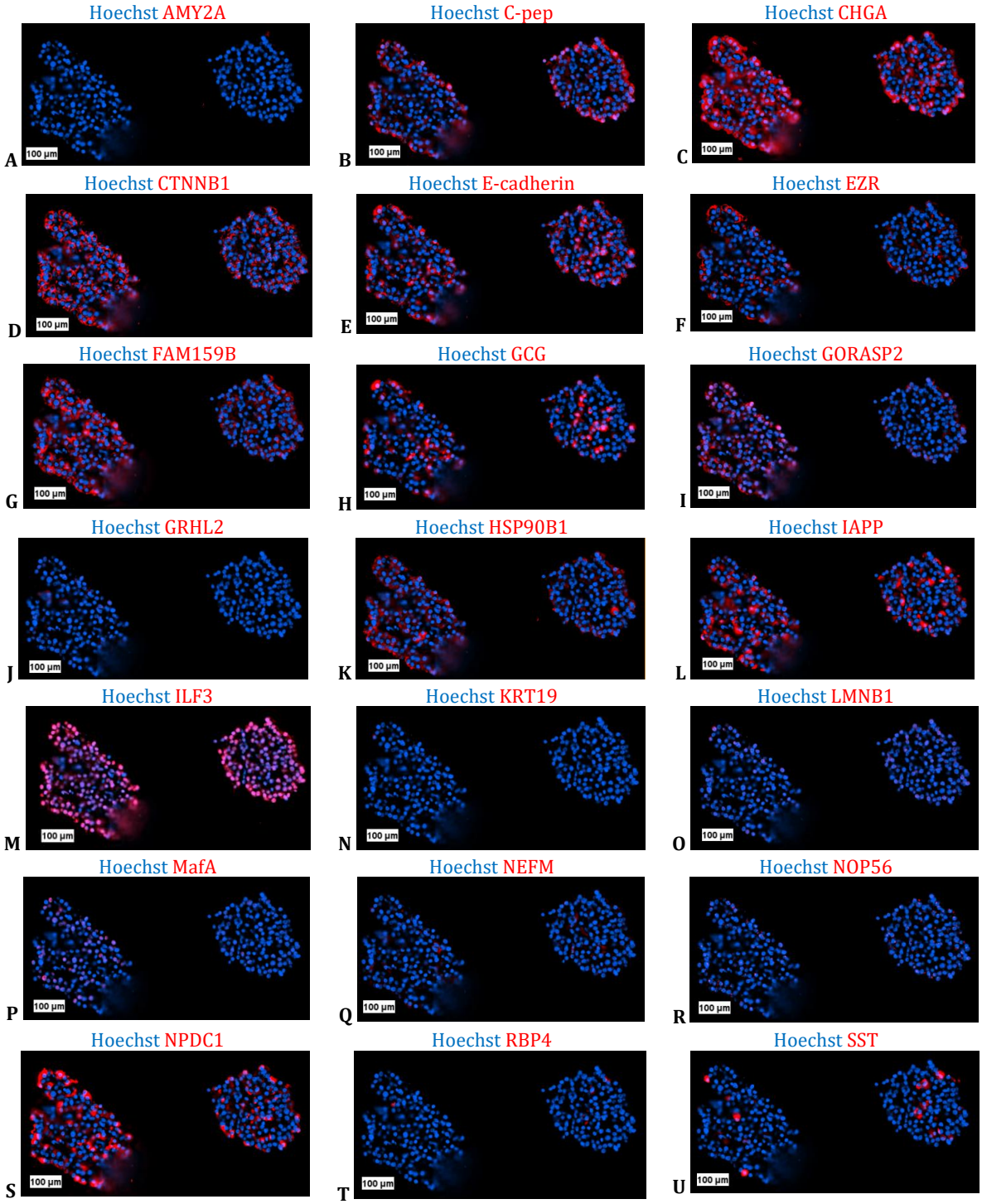

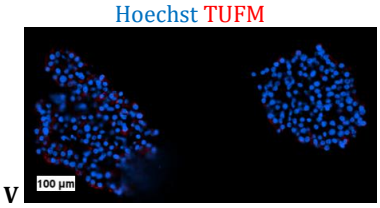

Figure 4. Immunostaining of each individual protein targeted by the 22-plex in-house conjugated antibody panel in isolated human pancreatic islets. The nuclei are visualized in blue (Hoechst) and the proteins are visualized in red.

To visually represent the generated multiplex data for each cell in the sample, tSNE-plots were produced, in which each marker was visualized individually to allow for identification of cell types within the tissue (Fig. 5A-V). It is observable that the organelle markers are homogenously expressed across all cells. Moreover, it is visible that there are variations in expression of the pancreatic markers in different regions in the plots, indicative of disparate cell populations. For example, it is noticeable that cells with a high expression of SST and RBP4 are separated from cells with a high expression of GCG. Furthermore, it can be observed that cells with a high expression of GCG and CHGA are in close proximity of each other and that there is a partial overlap of cells expressing these markers.

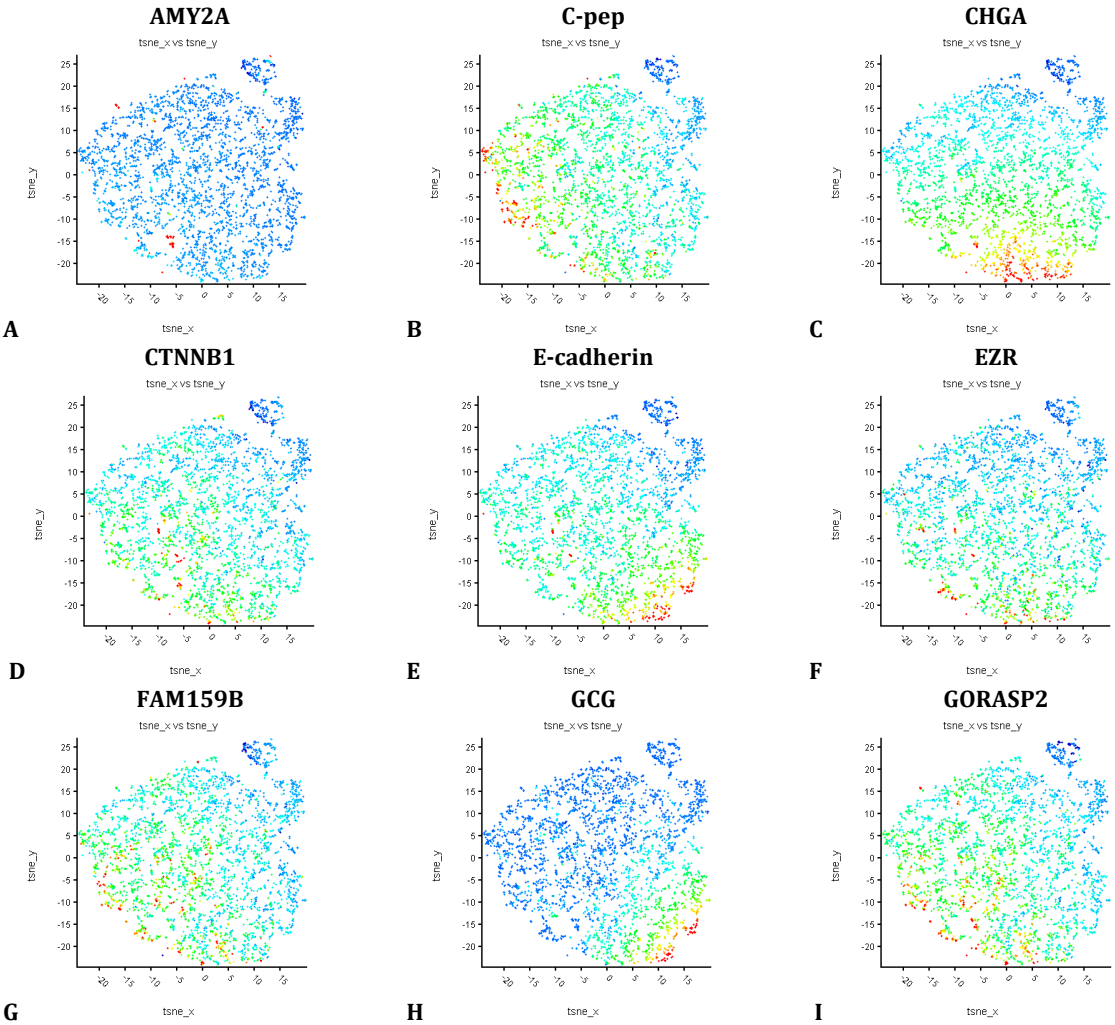

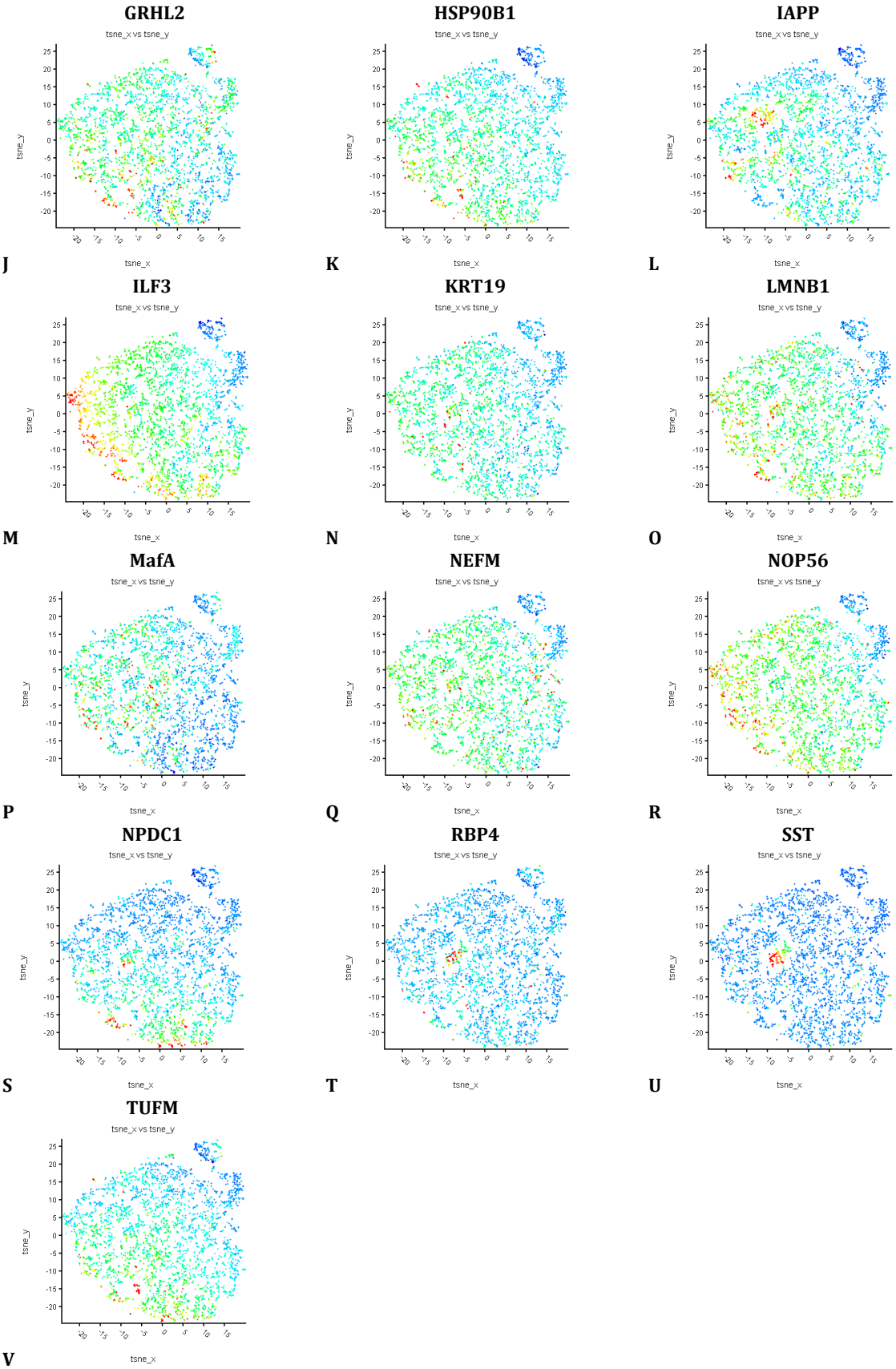

Figure 5. tSNE-plots of each individual marker in the 22-plex in-house conjugated antibody panel. Each dot represents a cell in the sample. Blue indicates low expression and red indicates high expression.

To investigate the different cell types within the sample, X-shift clustering was performed based on the expression of the 10 markers specifically expressed in pancreatic islets [21]. The clustering resulted in the

detection of 6 different populations. To analyse these populations further, a boxplot was generated to visualize the differences in marker expression of each population (Fig. 6). Notably, ILF3 appear to be highly expressed across all populations while MafA and RBP4 display low expression in all populations. Moreover, it is visible that Population 2 is the only population with a high expression of SST, clearly distinguishing it from the other populations. Furthermore, it can be observed that CHGA is highly expressed across all populations. However, it appears that CHGA is higher expressed in the populations that also have high expression of GCG, namely Population 3, 4 and 5. Additionally, C-pep appear to be expressed across all populations but seems to have a higher expression in the populations with low expression of GCG, i.e. population 1 and 6.

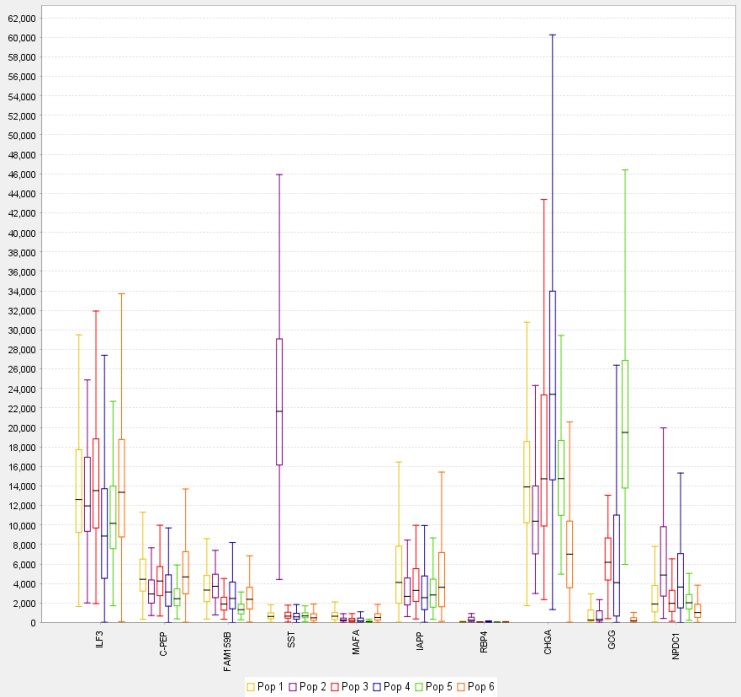

Figure 6. A comparison of signal intensities of the islet specific markers for each population identified by X-shift clustering.

To analyse the populations further, pancreatic markers that appeared to be differently expressed in the populations were visualized and overlapped (Fig. 7-11). Figure 7 displays the expression of five proteins in Population 1 and 6, where an overlap of high expression of C-pep, IAPP and FAM159B is visible. Moreover, the cells in Population 1 express both CHGA and ILF3, where ILF3 appear highly expressed and CHGA is less expressed compared to other cells within the islet. The difference between Population 1 and 6 appears to be that the cells within Population 6 has a lower expression of CHGA than Population 1.

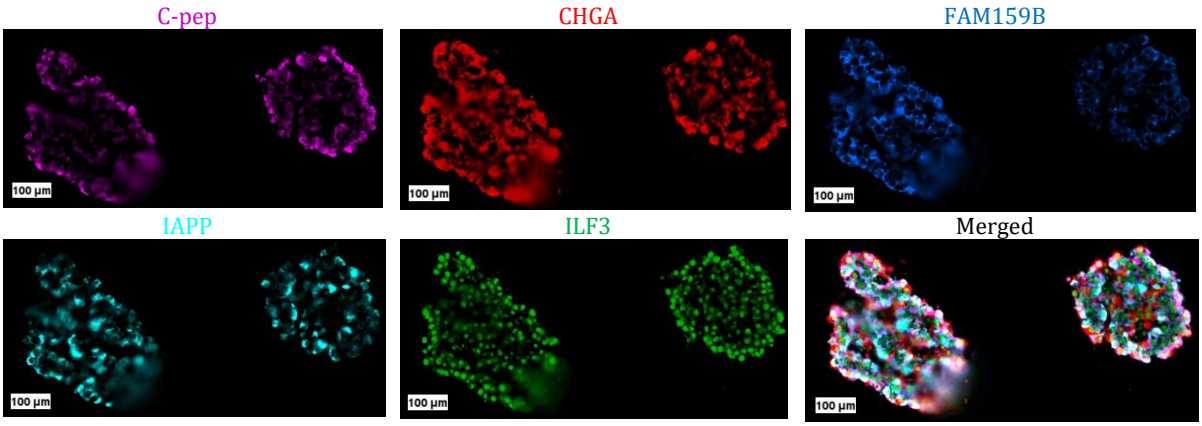

Figure 7. Immunostaining of five different proteins expressed in Population 1 and 6. C-peptide (C-pep) is showed in magenta, Chromogranin A (CHGA) in red, Shisa like 2B (FAM159B) in blue, Islet amyloid polypeptide (IAPP) in cyan, Interleukin enhancer binding factor 3 (ILF3) in green. The immunostaining of all five proteins is overlapped in the final image labelled "Merged".

In Figure 8, Population 2 is visualized through the expression of 6 proteins. Notably, there is an overlap of SST, RBP4 and NPDC1 in this population, while the cells also display expression of CHGA, FAM159B and ILF3. However, the signal from RBP4 is weak and the observed overlap is only partial for the SST positive population.

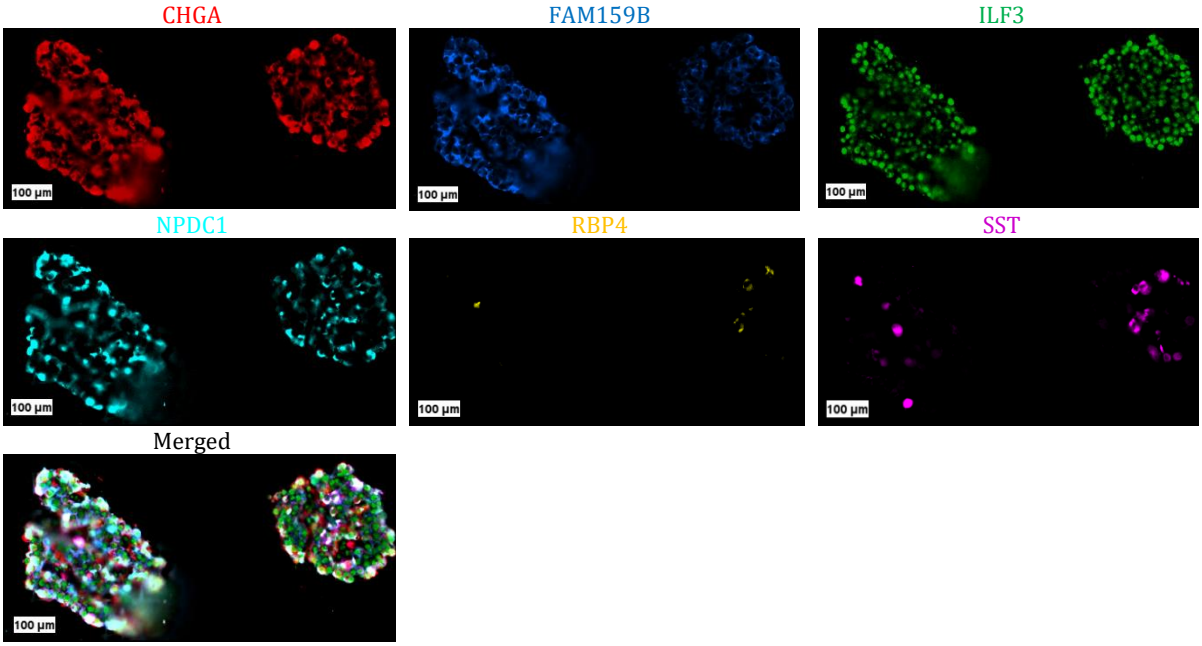

Figure 8. Immunostaining of six different proteins expressed in Population 2. Chromogranin A (CHGA) is showed in red, Shisa like 2B (FAM159B) in blue, Interleukin enhancer binding factor 3 (ILF3) in green, Neural proliferation, differentiation and control 1 (NPDC1) in cyan, Retinol binding protein 4 (RBP4) in yellow and somatostatin (SST) in magenta. The immunostaining of all six proteins is overlapped in the final image labelled "Merged".

Figure 9 shows the expression of five different proteins in Population 3. Here, both ILF3 and CHGA are highly expressed. Interestingly, there is an overlap of expression of GCG, C-pep and IAPP in this population.

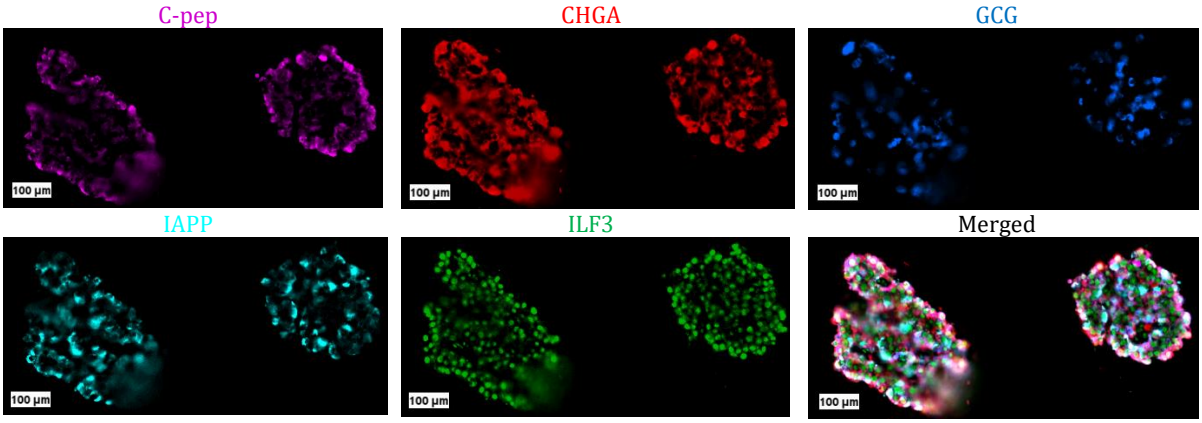

Figure 9. Immunostaining of five different proteins expressed in Population 3. C-peptide (C-pep) is showed in magenta, Chromogranin A (CHGA) in red, glucagon (GCG) in blue, Islet amyloid polypeptide (IAPP) in cyan and Interleukin enhancer binding factor 3 (ILF3) in green. The immunostaining of all five proteins is overlapped in the final image labelled "Merged".

In Figure 10, the expression of six proteins is on display to visualize Population 4. In this population, there is a high expression of CHGA. The cells with high expression of CHGA in Population 4 overlap with expression of FAM159B, ILF3, NPDC1, GCG and C-pep.

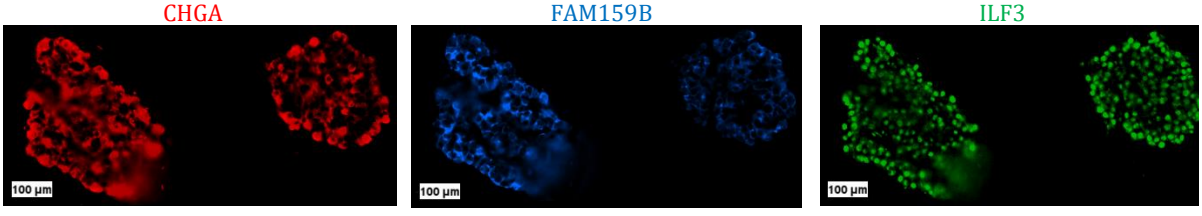

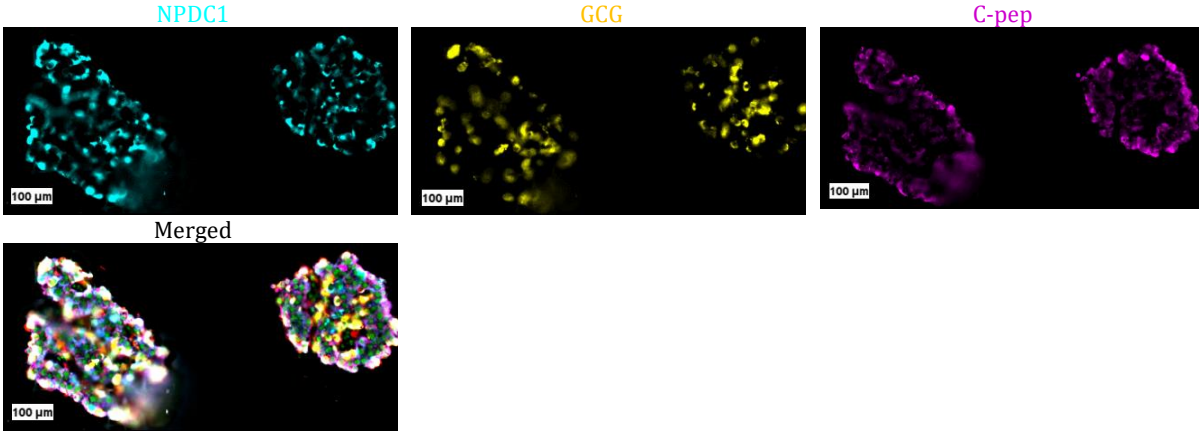

Figure 10. Immunostaining of six different proteins expressed in Population 4. Chromogranin A (CHGA) is showed in red, Shisa like 2B (FAM159B) in blue, Interleukin enhancer binding factor 3 (ILF3) in green, Neural proliferation, differentiation and control 1 (NPDC1) in cyan, glucagon (GCG) in yellow and C-peptide (C-pep) in magenta. The immunostaining of all six proteins is overlapped in the final image labelled "Merged".

In Figure 11, the expression of five proteins is on display to visualize Population 5. In this population, there appears to be an overlap of high expression of CHGA, NPDC1 and GCG. Yet, there is also expression of IAPP and ILF3.

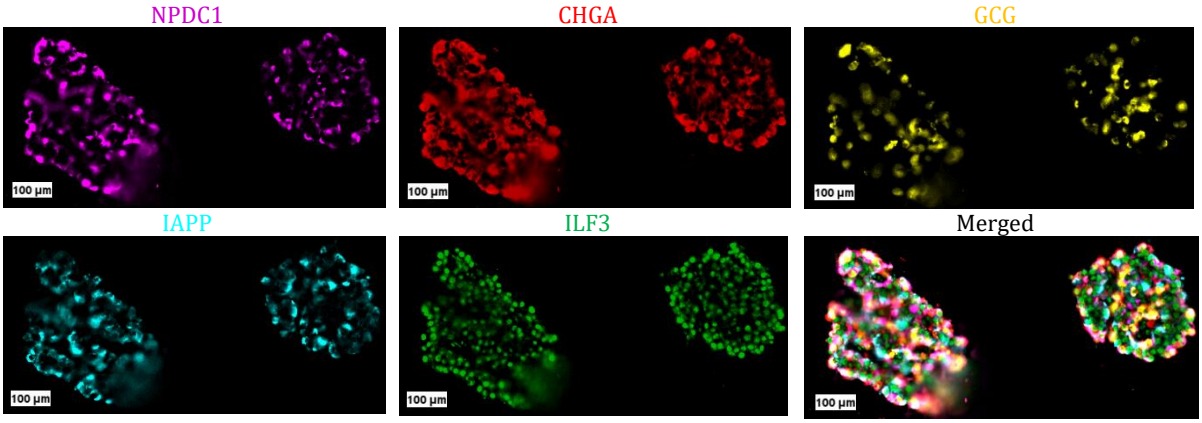

Figure 11. Immunostaining of five different proteins expressed in Population 5. Neural proliferation, differentiation and control 1 (NPDC1) is showed in magenta, Chromogranin A (CHGA) in red, glucagon (GCG) in yellow, Islet amyloid polypeptide (IAPP) in cyan and Interleukin enhancer binding factor 3 (ILF3) in green. The immunostaining of all five proteins is overlapped in the final image labelled "Merged".

Lastly, Voronoi diagrams were constructed to display how the different populations were distributed within the islets (Fig. 12A&B). In Figure 12A&B, it is visible that cellular composition between different islets in the sample vary greatly. Based on these limited number of samples, the islet cell population seem well-mixed, and no obvious topological organization can be observed. Additionally, it can be observed that the islet cell populations display both heterotypic and homotypic interactions within the samples.

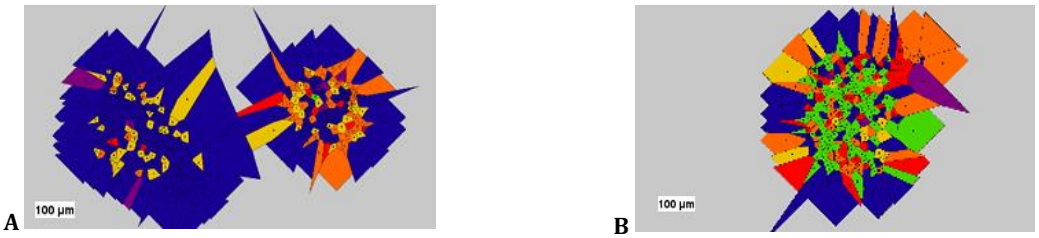

Figure 12. The cellular composition and organization of human isolated pancreatic islets illustrated by Voronoi diagrams. Population 1 is illustrated in yellow, Population 2 in purple, Population 3 in red, Population 4 in blue, Population 5 in green and Population 6 in orange. (A) Two pancreatic islets present within the isolated islets sample as marked by the white rectangle in Figure 3. (B) One pancreatic islet within the isolated islets sample.

Multiplex tissue imaging of pancreas tissue section

To image the pancreas tissue section a 22-plex panel of in-house DNA-barcode conjugated antibodies was used. 9 antibodies targeted proteins known to be specifically expressed in organelles of human cells, 1

targeted neurons and 12 targeted proteins specifically expressed in the pancreas (Appendix 4). The entire region of the pancreas tissue section that was imaged is presented in Figure 13 and consisted of 139,409 cells out of which 3,372 were identified to be endocrine cells. In Figure 13, the white rectangle displays which region of the tissue each marker has been visualized in Figure 14A-V.

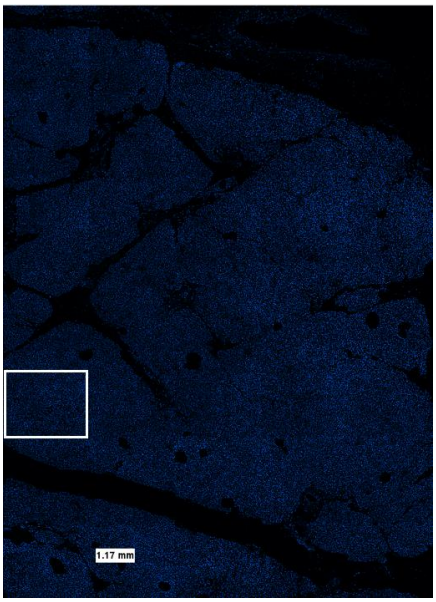

Figure 13. Sample overview of the region of the human pancreas tissue section that was imaged where the nuclei are visualised in blue (Hoechst).

In Figure 14A-V, each of the 22 proteins targeted by the multiplex antibody panel have been visualized. From the images it can be observed that there is no discernible staining pattern for either MafA or NEFM, indicating that these conjugated antibodies need to be optimized for multiplex imaging of pancreas tissue sections. Moreover, it is visible that the cytoplasmic staining of AMY2A in the acinar tissue is weak, suggesting that this conjugated antibody requires further evaluation. Additionally, cells that have a high expression of GCG and CHGA appear to be localized to the islet mantle. Furthermore, it visible the signal intensities vary between the cells within the islet of the pancreas specific markers, suggesting that these proteins are heterogeneously expressed.

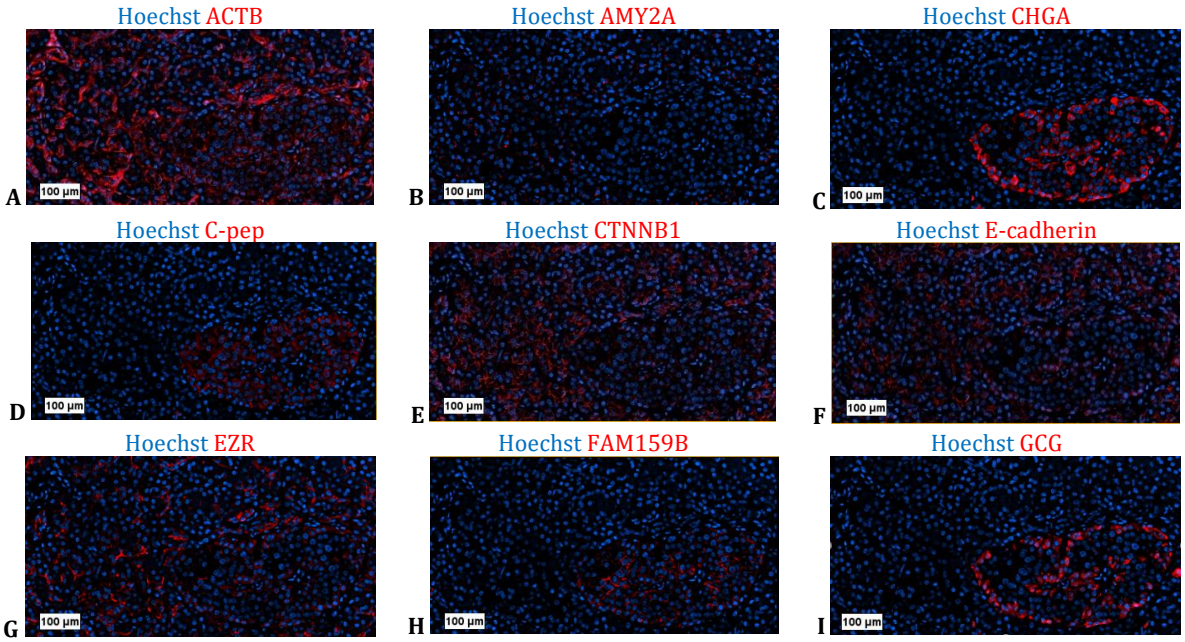

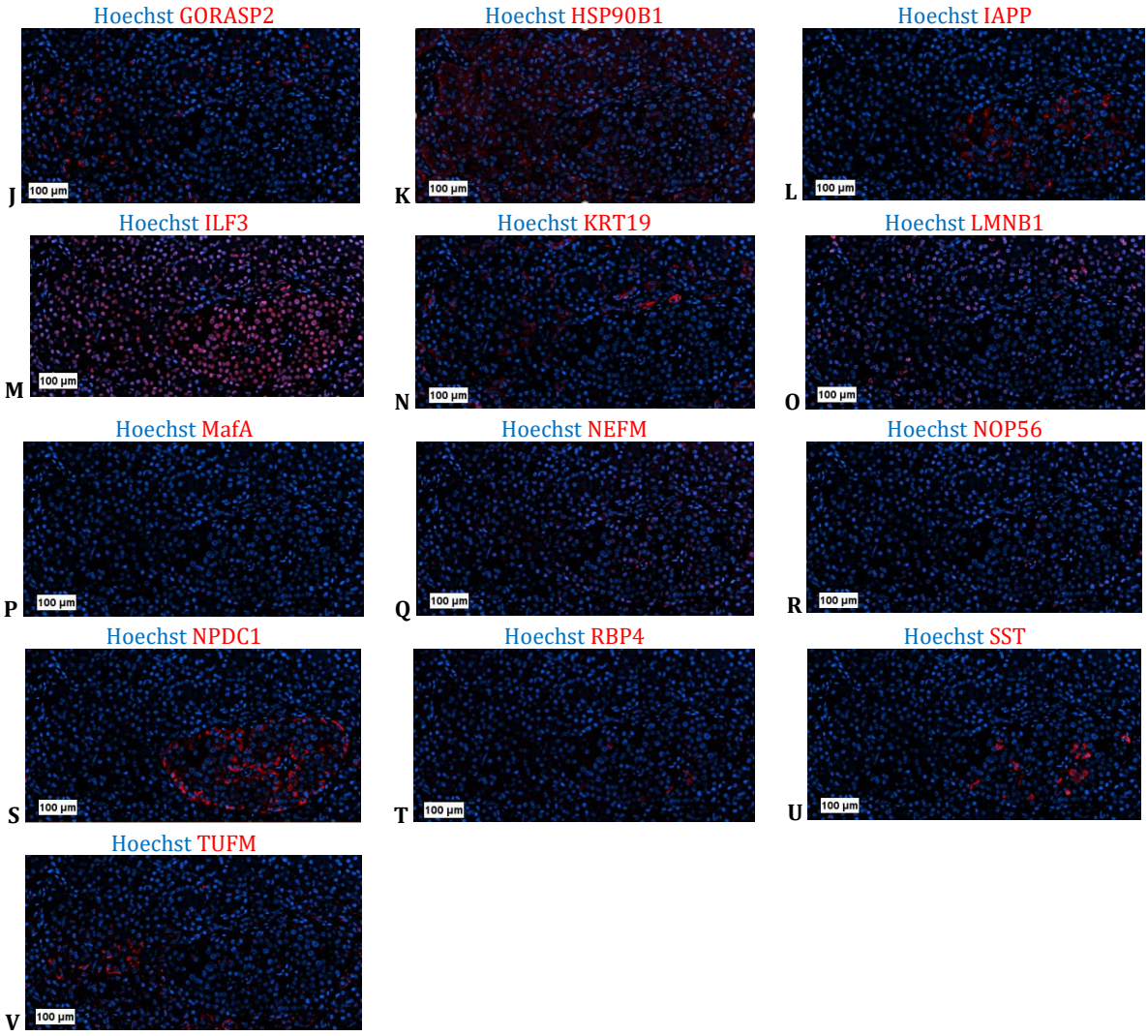

Figure 14. Immunostaining of each individual protein targeted in the 22-plex antibody panel in a human pancreas tissue section. The nuclei are visualized in blue (Hoechst) and the proteins are visualized in red.

tSNE-plots were produced to visually represent the generated high-dimensional multiplex data for each cell in the sample in which each marker was visualized individually to allow for identification of cell types within the tissue (Fig. 15A-V). It can be observed that the organelle markers predominantly are homogenously expressed across all cells in the sample. Furthermore, it is visible that the membrane markers CTNNB1, E-cadherin and EZR are highly expressed and localized in the same region of the plot together with the ductal marker KRT19. Notably, the islet specific markers appear to be highly expressed within the same region of the plot, distinct from the other cells in the sample.

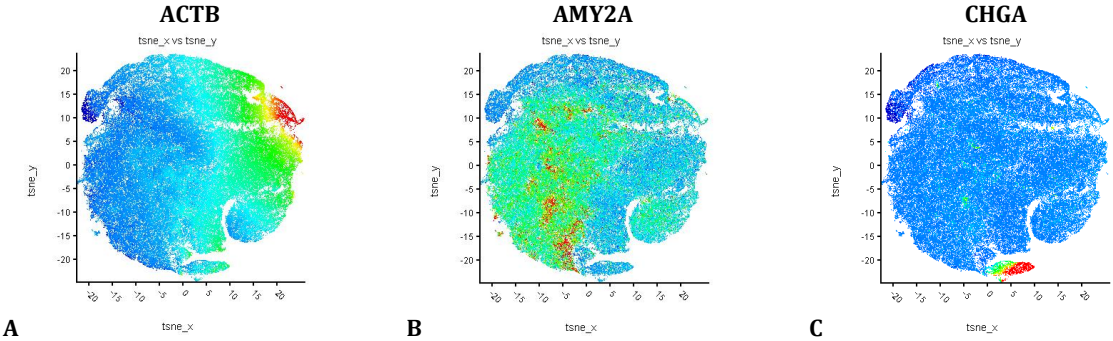

C-pep

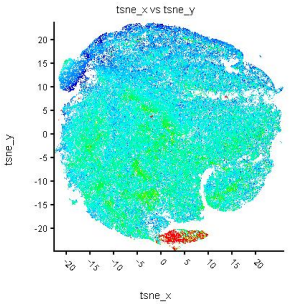

D

CTNNB1

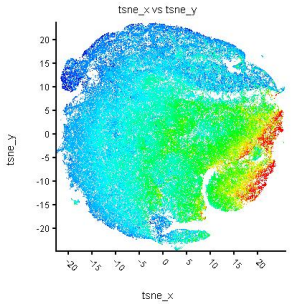

E

E-cadherin

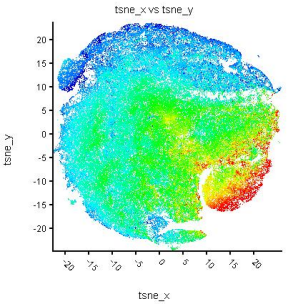

F

EZR

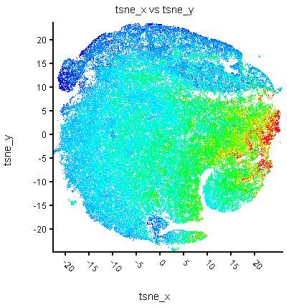

G

FAM159B

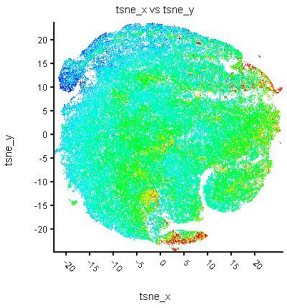

H

GCG

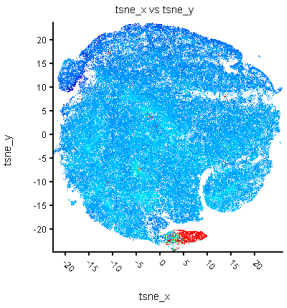

I

GORASP2

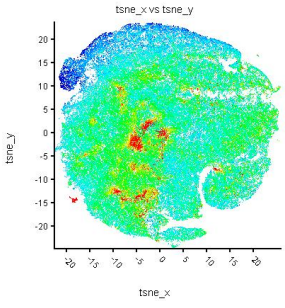

J

HSP90B1

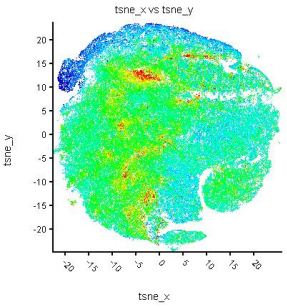

K

IAPP

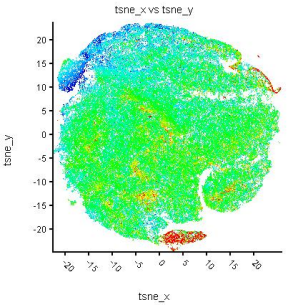

L

ILF3

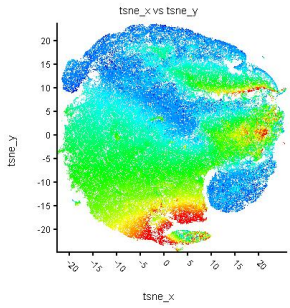

M

KRT19

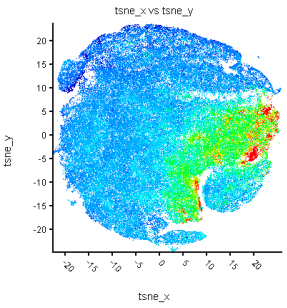

N

LMNB1

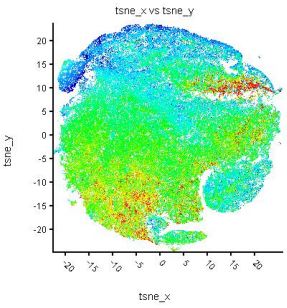

O

MafA

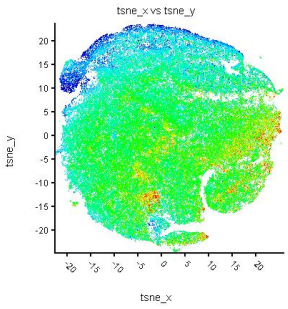

P

NEFM

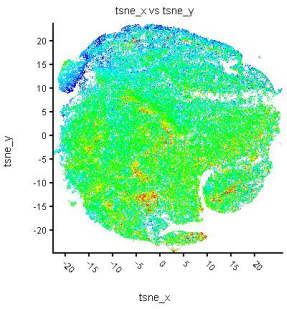

Q

NOP56

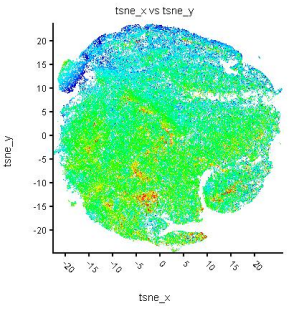

R

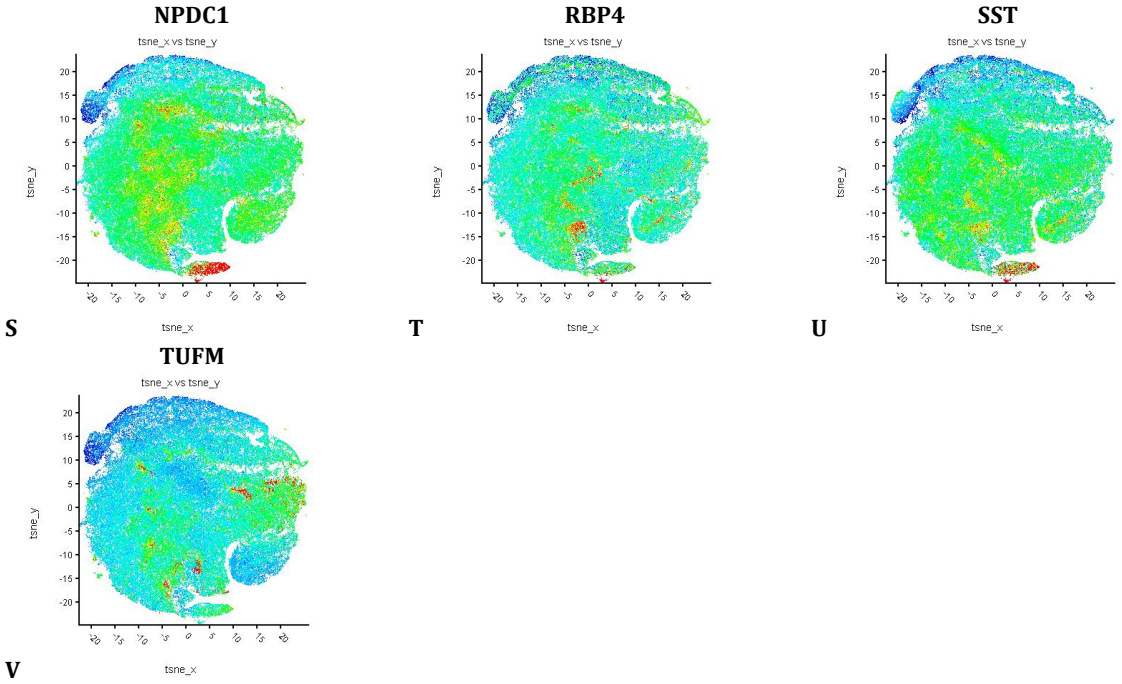

Figure 15. tSNE-plots of each individual marker in the 22-plex antibody panel. Each dot represents a cell in the sample. Blue indicates low expression and red indicates high expression.

As for the isolated islets, X-shift clustering was performed based on the expression of the 10 markers specifically expressed in pancreatic islets which yielded 29 different populations. However, it was found that only 1 of 29 populations specifically mapped to the pancreatic islets. Thus, to enable further analysis of what cell types were present in the pancreatic islets, the region of the tSNE-plots which displayed high expression of islet specific markers (Fig. 15A-V) was selected and magnified (Fig. 16A-J). In this view, it is visible that cells with high expression of GCG and CHGA largely are situated in the same region of the plot. Moreover, it can be observed that cells with a high expression of C-pep mainly are located to a different region than that of cells with a high expression of GCG and CHGA. However, there are still cells with high expression of C-pep that are overlapping with high expression of GCG and CHGA. Similarly, it can be observed that cells with a high expression of IAPP mainly appears to have a high expression of C-pep and that cells with a high expression of NPDC1 largely have a high expression of GCG.

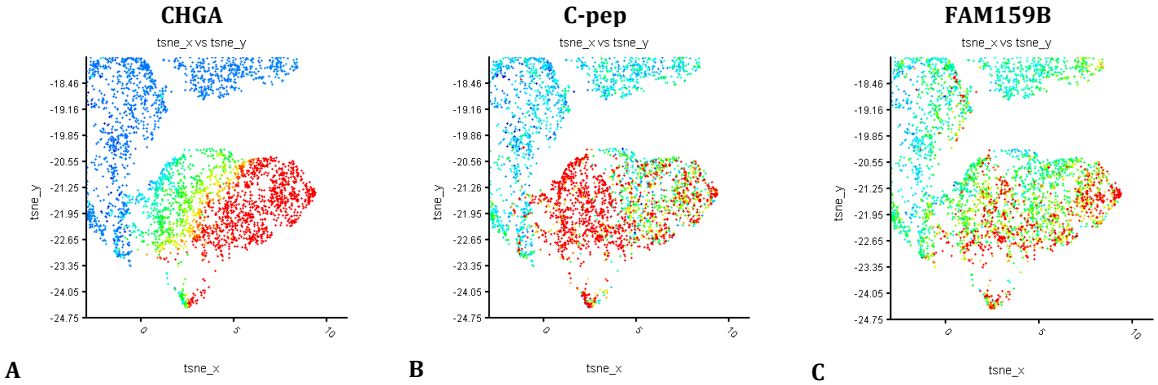

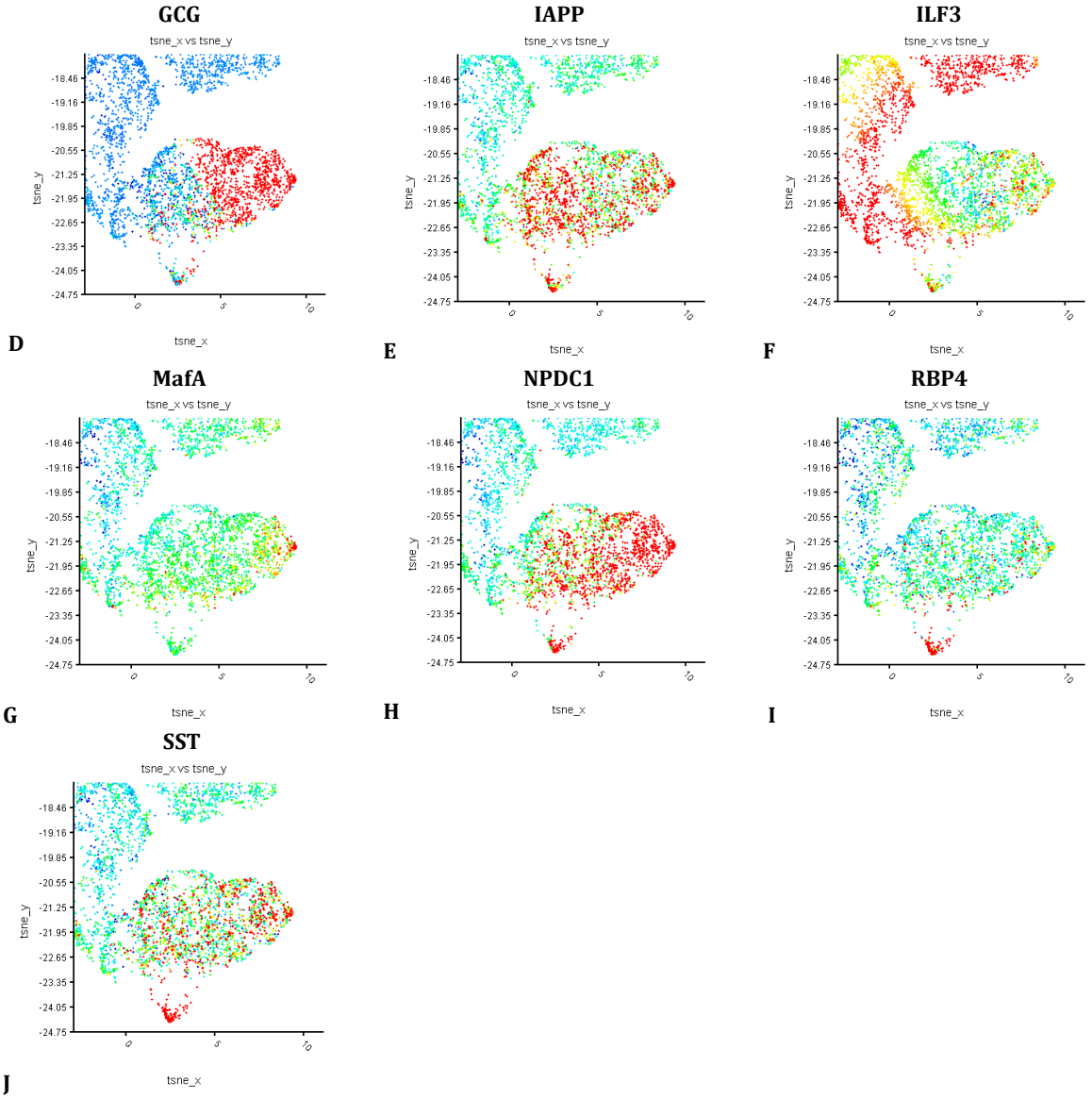

Figure 16. Magnified view of the region within the tSNE-plots in which there was high expression of the islet specific markers. Each dot represents a cell in the sample. Blue indicates low expression and red indicates high expression.

From Figure 16A-J, cell populations were created manually by gating cells that displayed a high expression of GCG, C-pep, CHGA and SST, respectively. To analyse the differences in marker expression further between these populations, a boxplot was generated (Fig. 17). It can be observed that ILF3 is highly expressed all populations while MafA and RBP4 display low signal intensity across all populations. For MafA, this was expected as there was no detectable staining present in the sample (Fig. 14M). RBP4 could be observed to have specific staining pattern, but the signal intensity is low in the acquired images, making it difficult to obtain any information about the cell populations based on the expression of RBP4 (Fig. 14T). Furthermore, it is visible that Population 3 is clearly distinguishable from the other populations based on its high expression of SST. Moreover, it can be observed that CHGA is highly expressed within the populations with a high expression of GCG, i.e. Population 1 and 2. Additionally, C-pep appear to be expressed across all populations, but with a marginally higher signal in one of populations that has a low expression of GCG, i.e. Population 4.

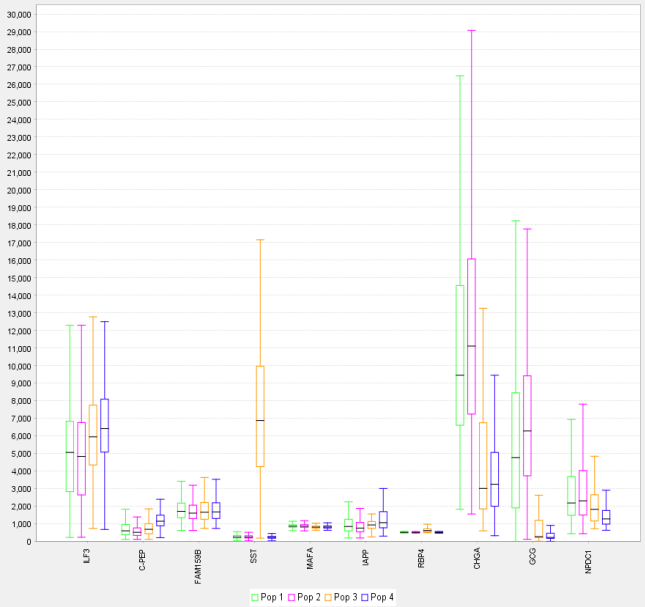

Figure 17. A comparison of signal intensities of the islet specific markers for each population identified by gating.

To analyse the disparities between the populations further, pancreatic markers that appeared to be differently expressed were individually visualized and overlapped (Fig. 18-20). In Figure 18 the expression of six proteins in Population 1 and 2 is displayed. In both populations, it is visible that cells with high expression of CHGA, NPDC1 and GCG overlap. Notably, it visible that Population 1 and 2 display very similar expression profiles and potential differences between the populations could be due to bias in the in the gating of the populations. Consequently, the populations were regarded as one population.

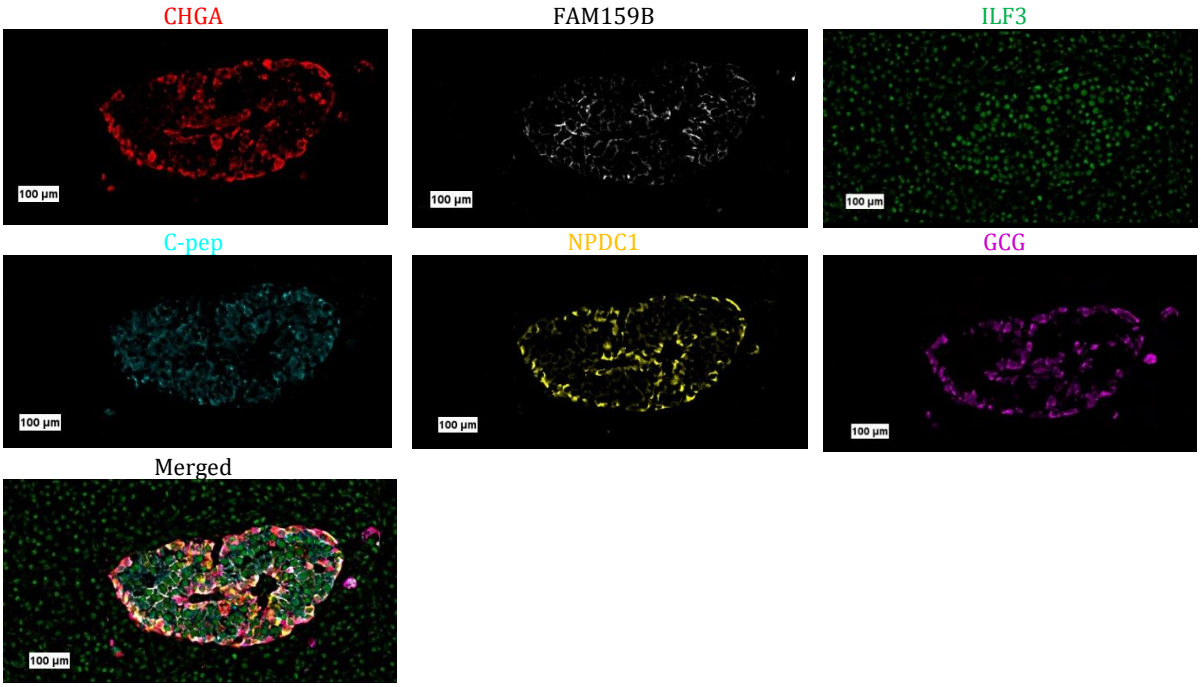

Figure 18. Immunostaining of six different proteins expressed in Population 1 and 2. Chromogranin A (CHGA) is showed in red, Shisa like 2B (FAM159B) in white, Interleukin enhancer binding factor 3 (ILF3) in green, C-peptide (C-pep) in cyan, Neural proliferation, differentiation and control 1 (NPDC1) in yellow and glucagon (GCG) in magenta. The immunostaining of all six proteins is overlapped in the final image labelled "Merged".

Figure 19 display the expression of seven proteins in Population 3. It is visible that cells with expression of SST in the population partly overlap with expression of CHGA, NPDC1 and FAM159B. Moreover, RBP4 appears to be expressed in STT positive cells since a partial overlap of the two markers can be observed.

However, the signal of RBP4 was low in the sample and therefore it is difficult to ascertain if this finding is valid or not.

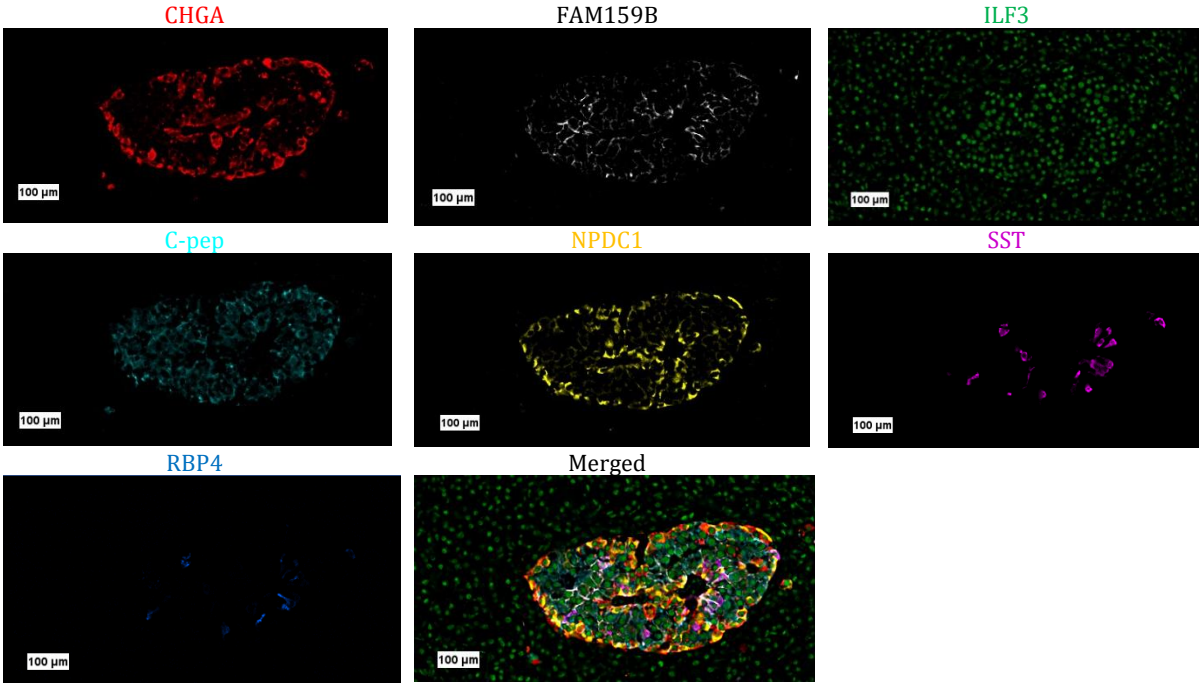

Figure 19. Immunostaining of seven different proteins expressed in Population 3. Chromogranin A (CHGA) is showed in red, Shisa like 2B (FAM159B) in white, Interleukin enhancer binding factor 3 (ILF3) in green, C-peptide (C-pep) in cyan, Neural proliferation, differentiation and control 1 (NPDC1) in yellow, somatostatin (SST) magenta and Retinol binding protein 4 (RBP4). The immunostaining of all seven proteins is overlapped in the final image labelled "Merged".

Five proteins expressed in Population 4 are visualized and overlapped in Figure 20. It can be observed that cells in Population 4 primarily express C-pep, ILF3, FAM159B and IAPP. There are also cells that are expressing CHGA in Population 4, but the expression of CHGA appears lower than that of the other populations.

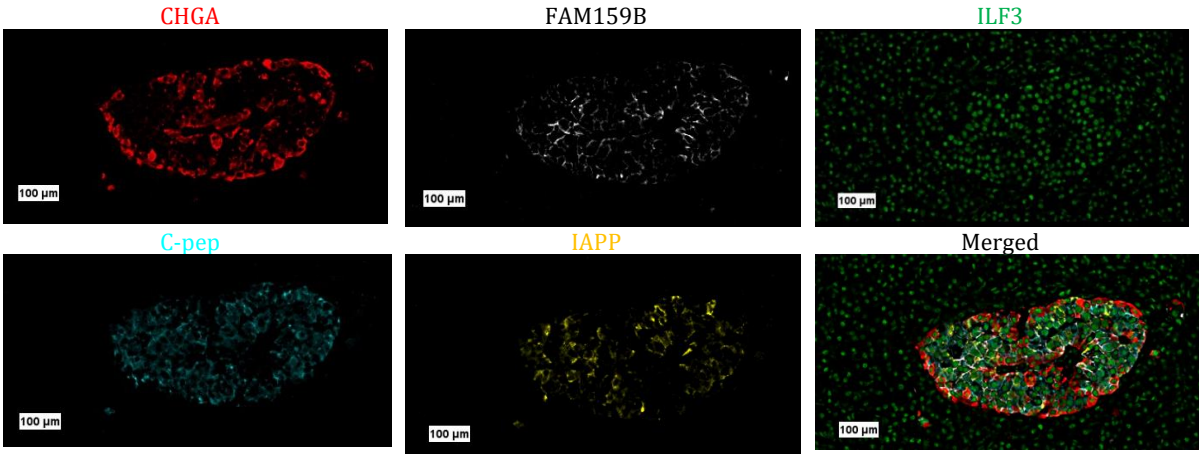

Figure 120. Immunostaining of five different proteins expressed in Population 4. Chromogranin A (CHGA) is showed in red, Shisa like 2B (FAM159B) in white, Interleukin enhancer binding factor 3 (ILF3) in green, C-peptide (C-pep) in cyan and Islet amyloid polypeptide (IAPP) in yellow. The immunostaining of all five proteins is overlapped in the final image labelled "Merged".

To study and visualize how the different populations were distributed within the islets, Voronoi diagrams were created (Fig. 21A&B). It is visible that cells in the combined population consisting of Population 1 and 2 are localizing to the same regions in the islets, i.e. the islet mantle and parts of the centre of the islet. Moreover, Population 4 is mainly localized to the centre of the islet. Additionally, both homotypic and heterotypic interactions between the different cells within the islet can be observed.

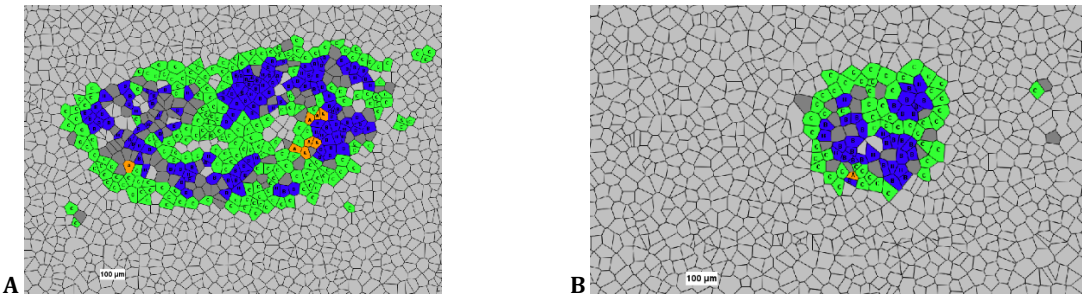

Figure 21. The cellular composition and organization of pancreatic islets in a human pancreas tissue section illustrated by Voronoi diagrams. (A) The combined population consisting of Population 1 and 2 is displayed in green, Population 3 in orange and Population 4 in blue for one islet in the sample. Cells marked in dark grey represent overlapping populations. (B) The combined population consisting of Population 1 and 2 is displayed in green, Population 3 in orange and Population 4 in blue for another islet in the sample. Cells marked in dark grey represent overlapping populations.

DISCUSSION

When comparing the multiplex imaging of the isolated pancreatic islets and the pancreas tissue section, there are some notable similarities and differences. First, it is visible that the organelle markers included in both antibody panels were homogenously expressed in the pancreatic islet cells. The opposite was observed for most proteins specifically expressed in islet cells since there was a visible difference in signal intensity between cells in the islets. This corroborates previous studies where islet cells have been found to display heterogeneity as well as the findings of the collaborative project. Furthermore, supporting the results of the collaborative project, it could be observed that IAPP mainly was expressed in cells that displayed expression of C-pep and not in cells that expressed GCG, corroborating previous studies of the expression of IAPP in islet cells [22]. NPDC1 was primarily observed to be highly expressed in cells that had a high expression of GCG, indicating that NPDC1 can play an important role in the function of GCG positive cells. Additionally, cells that had a high expression of SST overlapped with cells that expressed NPDC1, suggesting that NPDC1 also may be important for the function of SST positive cells. Moreover, FAM159B was observed to display a higher expression in cells with a high expression of C-pep and SST than in cells expressing GCG, indicating that FAM159B may be of functional importance for both C-pep and SST positive cells. Furthermore, high expression of CHGA was observed to predominantly overlap with cells that displayed high expression of GCG comparative to cells expressing C-pep. Interestingly, other studies that have explored the expression of CHGA in islets cells have revealed that CHGA can be processed into multiple different bioactive peptides such as pancreastatin and chromostatin. A study that investigated the immunoreactivity of different antibodies toward CHGA found that most commercially available antibodies have been developed to target the entire length of CHGA, meaning that it the antibody will bind to the full-length protein as well as its bioactive peptides [23]. The antibody used to target CHGA in this study (NBP2-34674) is developed toward the full-length protein. Thus, to be able to study if there is a difference in expression between the bioactive peptides, and their potential functional disparities within islets cells, other more specific antibodies need to be used. Moreover, this study revealed that ILF3 was homogenously expressed in the nuclei of all islet cells, opposing the collaborative project's finding that ILF3 was highly expressed in β-cells.

In addition to the marker expression in the different islet cells, the structure of the islets in the different samples were studied. Comparing the isolated pancreatic islets with the islets in the pancreas tissue section, there is a notable difference in the organization of cells. In the isolated islets, no apparent internal organization could be observed as the different populations of cells were seemingly well-mixed the islets. The islets in the pancreas tissue section did, however, display an internal organization where cells with a high expression of GCG mainly localized to the islet mantle and cells with expression of C-pep were located to the centre of the islet. These observations need to be further investigated in multiple samples from different donors and different regions of the pancreas to determine if this something that can be observed across donors or if islets tend to have distinct structures in different regions of the pancreas.

The screened and conjugated antibodies targeting MafA and RBP4 illustrates some of the challenges associated with multiplex tissue imaging via antibody staining. Despite displaying target specificity and high SNR when detected through indirect immunofluorescence, both antibodies showed a decrease in signal when detected through direct immunofluorescence. Using the detection of the barcode-reporter binding event, the signal is weaker than when using indirect immunofluorescence where the signal is amplified by

the secondary antibody. By increasing the concentration of the conjugated anti-MafA antibody in the multiplex tissue imaging, MafA could be visualized in the isolated pancreatic islets but not in the pancreas tissue section. Though a specific staining pattern could be observed in the isolated pancreatic islets, the signal was still too low to allow for further downstream analysis. RBP4 could be detected in both samples, but the signal was also too low for this marker to allow for further analysis. The anti-RBP4 antibody had first been screened using Cy5, a far-red fluorophore, where a specific staining pattern and high SNR was observed. Subsequently, it was screened using Cy7, a near-infrared fluorophore, where it maintained high SNR (Fig. 1B). However, when conjugated with a DNA-barcode complementary to a DNA-reporter labelled with Cy7, the SNR decreased. Cameras are less sensitivity in the near-infrared spectrum, leading to a less strong signal for near-infrared fluorophores compared to other available fluorophores. Subsequently, the anti-RBP4 antibody could be conjugated with a different barcode detectable with another fluorophore to allow for further analysis of the expression of RBP4 in islet cells and potentially validate the observed overlap of expression of SST and RBP4. Additionally, when comparing the tissue staining of the validated conjugated anti-C-peptide (C-pep) antibody with the multiplex tissue imaging, it is visible that there is a difference between the two staining patterns. In the validation of the conjugated antibody, the staining is limited to a few cells within the islets while the staining is visible throughout the islets in the multiplex tissue imaging (Fig. 2B, 4B & 14D). This indicates that the conjugated antibody needs to be further evaluated to ensure retained target specificity in multiplex tissue imaging. Consequently, there are multiple challenges with multiplex tissue imaging through the CODEX platform that have been exemplified in this study. The assay is heavily dependent on antibody specificity, requiring each antibody to be thoroughly tested prior to conjugation, after conjugation as well as in multiplex tissue imaging to evaluate its performance in each instance. Furthermore, it is limited by the use of direct immunofluorescence since less abundant proteins potentially cannot be detected in the tissue.

The developed technologies for multiplex tissue imaging available today are highly advanced and generates vast amounts of data that hold great promise for gaining a deepened understanding of cell biology in health and disease. However, there is currently a lack of precise and accessible tools for processing and downstream analysis of the data that is generated which is limiting what information that can be acquired [24, 25]. One area that is posing a particular challenge is the cell segmentation. Aforementioned, cell segmentation is the process in which the boundaries of each individual cell within the image of the tissue are set and allows for analysis of protein expression at the single cell level. Tissues are intricate structures composed multiple different cell types with varying morphologies, making it difficult for one cell segmentation algorithm to accurately predict the boundary of each individual cell within one image. Example images of the cell segmentation predicted by the CODEX® Processor in the isolated islets and pancreas tissue section can be viewed in Appendix 6. From these images it can be observed that there are instances of both hyper- and hyposegmentation as some cells lack boundaries whilst others have been predicted to being more than one cell. These erroneously identified and missed cells have a direct impact on the downstream analysis, especially in datasets consisting of rare cell types. In this study, the cell segmentation was deemed acceptable, however there is a need for improved cell segmentation algorithms to increase the accuracy of the downstream analysis as well as for different analysis tools that allow for comprehensive data analysis of the tissue microenvironment.

CONCLUSION

In this study, a multiplex imaging assay was constructed to simultaneously study 22 proteins in healthy human pancreatic islets using the CODEX platform for multiplex tissue imaging. Of the 22 studied proteins, 10 were specifically expressed in pancreatic islets and most were demonstrated to be heterogeneously expressed in different islet cells. The obtained results suggest that multiplex tissue imaging has the potential to generate a spatially resolved map of the healthy islet microenvironment. The generation of a spatially resolved map of the healthy islet microenvironment will improve the current understanding of islet cell functionality. Furthermore, mapping protein localization, distribution and dynamics in healthy human islets has the potential to become a valuable asset for biological and medical research by serving as a reference in future studies of several pancreatic diseases and disorders.

FUTURE PERSPECTIVES

The primary aim of this study was to build and validate the multiplex assay to visualize, analyse and annotate cell types in healthy human pancreatic islets using the CODEX platform for multiplex tissue imaging. In this study, only a small fraction of the proteomic targets identified by the collaborative project were studied due to time constraint. Based on the successful outcome of this work, a future objective would be to expand the library of in-house conjugated antibodies to include most of the identified protein targets and expand the assay to simultaneously visualize 40 target proteins. Furthermore, to be able to generate a map of the healthy human microenvironment, the protein targets would need to be studied in multiple different tissue samples to discover commonalities and differences in healthy human islet cells. Moreover, the development of new and improved tools for image processing and downstream data analysis would be encouraged to improve the accuracy of cell phenotyping. Additionally, it would be beneficial to use alternative methods for proteomic profiling of islet cells to validate the findings of this study as well as future studies.

ACKNOWLEDGEMENTS

I would like to express my deepest gratitude toward Emma Lundberg for generously giving me the opportunity to realize my dream to work on a project in spatial proteomics and for her continuous support, invaluable feedback, and constant encouragement. Furthermore, I am grateful toward my examiner Patrik Ståhl for his supervision of my master's degree project and for answering any of my doubts. Moreover, I would like to express my gratitude toward Hanna Tegel and Gabriella Jensen at the HPA project at the AlbaNova University Centre for supplying my project, and the Cell Profiling group, with antibodies. Additionally, I would like to express my sincerest thanks toward the Cell Profiling group for providing such a wonderful working environment and for always giving a helping hand whenever it was needed. Finally, I would like to thank my co-supervisor Anna Martinez Casals for going above and beyond making my experience with the project the absolute best and for her astonishing dedication, exceptional mentoring, extraordinary patience, kindness, and humour.

REFERENCES

1. The Human Protein Atlas. (2016). *Pancreas*. Retrieved from: The Human Protein Atlas Homepage: https://www.proteinatlas.org/learn/dictionary/normal/pancreas

2. The Human Protein Atlas. (2016). *The pancreas-specific proteome*. Retrieved from: The Human Protein Atlas Homepage: https://www.proteinatlas.org/humanproteome/tissue/pancreas

3. Da Silva Xavier, G. (2018). The Cells of the Islets of Langerhans. *Journal of Clinical Medicine*, 54.

4. Abdulreda, M. H., Rodriguez-Diaz, R., Cabrera, O., Caicedo, A. & Berggren, P. O. (2016). The Different Faces of the Pancreatic Islet. (eds) M. Ramírez-Domínguez, *Pancreatic Islet Isolation* (pp. 11-24). Springer, Cham. doi: https://doi.org/10.1007/978-3-319-39824-2_2

5. Cabrera, O., Berman, D. M., Kenyon, N. S., Ricordi, C., Berggren, P. O., & Caicedo, A. (2006). The unique cytoarchitecture of human pancreatic islets has implications for islet cell function. *Proceedings of the National Academy of Sciences of the United States of America*, *103*(7), 2334–2339. doi: https://doi.org/10.1073/pnas.0510790103

6. Bosco, D., Armanet, M., Morel, P., Niclauss, N., Berney, T., *et al* (2010). Unique Arrangement of α- and β-Cells in Human Islets of Langerhans. *Diabetes*, 1202-1210. doi: https://doi.org/10.2337/db09-1177

7. Brereton, M., Vergari, E., Zhang, Q., & Clark, A. (2015). Alpha-, Delta- and PP-cells: Are They the Architectural Cornerstones of Islet Structure and Co-ordination? *Journal of Histochemistry & Cytochemistry*, 575-591. doi: 10.1369/0022155415583535

8. Arrojo e Drigo, R., Roy, B. & MacDonald, P. E. (2020). Molecular and functional profiling of human islets: from heterogeneity to human phenotypes. *Diabetologia*, 2095–2101.

9. Avrahami, D., Klochendler, A., Dor, Y., & Glaser, B. (2017). Beta cell heterogeneity: an evolving concept. *Diabetologia*, 1363–1369. doi: https://doi.org/10.1007/s00125-017-4326-z

10. Avrahami, D., Wang, Y. J., Klochendler, A., Dor, Y., Glaser, B., & Kaestner, K. H. (2017). β-Cells are not uniform after all-Novel insights into molecular heterogeneity of insulin-secreting cells. *Diabetes, Obesity & Metabolism*, 147-152. doi: 10.1111/dom.13019

11. Teo, A. K. K., Lim, C. S., Cheow, L. F., Kin, T., Shapiro, J. A., *et al*, (2018). Single-cell analyses of human islet cells reveal de-differentiation signatures. *Cell Death Discovery*. doi: https://doi.org/10.1038/s41420-017-0014-5

12. Camunas-Soler, J., Dai, X.-Q., Hang, Y., Bautista, A., MacDonald, P. E., *et al*, (2020). Patch-Seq Links Single-Cell Transcriptomes to Human Islet Dysfunction in Diabetes. *Cell Metabolism, 31*, 1-15.

13. Thul, P. J. *et al.* A subcellular map of the human proteome. *Science* (2017), *356*(6340).

14. Lundberg, E., & Borner, G. H. (2019). Spatial proteomics: a powerful discovery tool for cell biology. *Nature Reviews Molecular Cell Biology*, 285-302.

15. Christopher, J.A., Stadler, C., Martin, C.E. *et al.* Subcellular proteomics. *Nat Rev Methods Primers* 1**,** 32 (2021). https://doi.org/10.1038/s43586-021-00029-y

16. Kennedy-Darling, J., Bhate, S. S., Hickey, J. W., Black, S., Nolan, G. P., *et al* (2021). Highly multiplexed tissue imaging using repeated oligonucleotide exchange reaction. *European Journal of Immunology*, 1262-1277. doi: 10.1002/eji.202048891

17. Tan, W., Nerurkar, S. N., Cai, H. Y., Ng, H., Wu, D., Wee, Y., Lim, J., Yeong, J., & Lim, T. (2020). Overview of multiplex immunohistochemistry/immunofluorescence techniques in the era of cancer immunotherapy. *Cancer communications (London, England)*, *40*(4), 135–153. doi: https://doi.org/10.1002/cac2.12023

18. Akoya Biosciences. (2020). *CODEX: A Comprehensive Solution for Spatially Resolved, Multiplexed Immunofluorescence*. Retrieved from: https://www.akoyabio.com/codex/

19. Schürch, C. M., Bhate, S. S., Barlow, G. L., Samusik, N., Goltsev, Y., & Nolan, G. P. (2020). Coordinated Cellular Neighborhoods Orchestrate Antitumoral Immunity at the Colorectal Cancer Invasive Front. *Cell*, 1-19

20. Uhlén, M. *et al* (2015). Tissue-based map of the human proteome. *Science (New York, N.Y.)*, *347*(6220), 1260419. doi: https://doi.org/10.1126/science.1260419

21. Samusik, N., Good, Z., Spitzer, M. H., Davis, K. L., & Nolan, G. P. (2016). Automated mapping of phenotype space with single-cell data. *Nature methods*, *13*(6), 493–496. doi: https://doi.org/10.1038/nmeth.3863

22. Westermark, P., Andersson, A., & Westermark, G. T. (2011). Islet amyloid polypeptide, islet amyloid, and diabetes mellitus. *Physiological reviews*, *91*(3), 795–826. doi: https://doi.org/10.1152/physrev.00042.2009

23. Portela-Gomes, G. M., & Stridsberg, M. (2001). Selective Processing of Chromogranin A in the Different Islet Cells in Human Pancreas. *Jounal of Histochemistry & Cytochemistry*. doi:https://doi.org/10.1177/002215540104900408

24. Stoltzfus, C. R., Filipek, J., Gern, B. H., Olin, B. E., Gerner, M. Y., *et al* (2020). CytoMAP: A Spatial Analysis Toolbox Reveals Features of Myeloid Cell Organization in Lymphoid Tisssues. *Cell Reports*.

25. Schapiro, D., Sokolov, A., Yapp, C., Muhlich, J. L., Hess, J., Lin, J. R., . . . Sorger, P. (2021). MCMICRO: A scalable, modular image-processing pipeline for multiplexed tissue imaging. *bioRxiv*. doi: https://doi.org/10.1101/2021.03.15.435473

APPENDIX

Appendix 1: Table presenting all screened commercial antibodies and their respective tested dilutions.

Target protein	Target gene	Antibody Cat#	Manufacturer	Antibody clonality	Dilution(s)
Chromogranin C	CHGC	GTX115049	GeneTex	Rabbit polyclonal, IgG	1:10
MAF bZIP transcription factor A	MafA	ab26405	Abcam	Rabbit polyclonal, IgG	1:25
MAF bZIP transcription factor A	MafA	ab272324	Abcam	Rabbit monoclonal, IgG	1:100
MAF bZIP transcription factor A	MafA	ab264418	Abcam	Rabbit monoclonal, IgG	1:100 and 1:200
NK6 homeobox 1	NKX6-1	ab268088	Abcam	Mouse monoclonal, IgG	1:50
Pancreatic and duodenal homeobox 1	PDX1	MAB2419-SP	R&D Systems	Mouse monoclonal, IgG	1:50 and 1:20
Progesterone receptor	PGR	14-9764-82	ThermoFisher Scientific	Mouse monoclonal, IgG	1:50
Retinol binding protein 4	RBP4	ab248553	Abcam	Rabbit monoclonal, IgG	1:100
Retinol binding protein 4	RBP4	ab226137	Abcam	Rabbit monoclonal, IgG	1:100 and 1:200
Solute carrier family 30 member 8	SLC30A8	MAB7936	R&D Systems	Mouse monoclonal, IgG	1:10

Appendix 2: Equation used for the determination of signal to noise ratio (SNR). $<I_{signal}>$ represent the mean pixel intensity of the 16-bit grey scale image for the regions in the image that show positive antibody staining. $<I_{background}>$ represent the mean pixel in of the 16-bit grey scale image for the regions in the image that show negative antibody staining.

$$SNR = \frac{< I_{signal} >}{< I_{background} >}$$

Appendix 3: Table presenting the HPA antibodies that were conjugated without prior screening through indirect immunofluorescence and the commercial antibodies that had been screened before the start of the master thesis project.

Target protein	Target gene	Antibody Cat#	Manufacturer	Antibody clonality
Aristaless related homeobox	ARX	MABN102	Sigma-Aldrich	Mouse monoclonal, IgG
Insulin	C-peptide	MA1-19159	ThermoFisher Scientific	Mouse monoclonal, IgG
Shisa like 2B	FAM159B	HPA011778	HPA	Rabbit polyclonal, IgG
Islet amyloid polypeptide	IAPP	HPA053194	HPA	Rabbit polyclonal, IgG
Interleukin enhancer binding factor 3	ILF3	HPA001897	HPA	Rabbit polyclonal, IgG
Cytokeratin 19	KRT19	ab7754	Abcam	Mouse monoclonal, IgG
Neural proliferation, differentiation and control 1	NPDC1	HPA008189	HPA	Rabbit polyclonal, IgG

Appendix 4: The two tables present the antibody panels used for the pancreas tissue section and isolated islets, respectively.

CODEX Antibody panel for multiplex tissue imaging of pancreas tissue section							
Target protein	**Target gene**	**Marker**	**Antibody Cat#**	**Manufacturer**	**Barcode**	**Reporter**	**Dilution**
Actin beta	ACTB	Beta actin	AMAb91241	Atlas Antibodies	BX024	RX024-Cy5	1:50
Amylase, alpha 2A (pancreatic)	AMY2A	Pancreatic amylase	PA5-50358	Thermo Fisher	BX010	RX010-Cy7	1:100
Chromogranin A	CHGA	Neuroendocrine marker	NBP2-34674	Novus Biologicals	BX006	RX006-Cy5	1:100
Insulin	C-peptide	Beta cells	MA1-19159	Thermo Fisher	BX047	RX047-Atto550	1:50
Catenin beta 1	CTNNB1	Cell junctions	AMAb91209	Atlas Antibodies	BX033	RX033-Cy5	1:50
E-cadherin	CDH1	Cell adhesion	PN 4250021	Akoya Biosciences	BX014	RX014-Atto550	1:100
Ezrin	EZR	Plasma membrane	AMAb90976	Atlas Antibodies	BX036	RX036-Cy5	1:100
Shisa like 2B	FAM159B	Beta cells	HPA011778	HPA	BX054	RX054-Cy5	1:25
Glucagon	GCG	Alpha cells	MAB12491	R&D Systems	BX032	RX032-Atto550	1:100
Golgi reassembly stacking protein 2	GORASP2	Golgi apparatus	AMAb91016	Atlas Antibodies	BX027	RX027-Cy5	1:50
Heat shock protein 90 beta family member 1	HSP90B1	ER	AMAb91019	Atlas Antibodies	BX030	RX030-Cy5	1:50
Islet amyloid polypeptide	IAPP	Beta cells	HPA053194	HPA	BX005	RX005-Atto550	1:100
Interleukin enhancer binding factor 3	ILF3	Beta cells	HPA001897	HPA	BX041	RX041-Atto550	1:100
Keratin 19	KRT19	Ductal cells	ab7754	Abcam	BX035	RX035-Atto550	1:100
Lamin B1	LMNB1	Nuclear membrane	AMAb91251	Atlas Antibodies	BX026	RX026-Atto550	1:50
MAF bZIP transcription factor A	MafA	Beta cells	ab264418	Abcam	BX042	RX042-Cy5	1:25
Neurofilament medium	NEFM	Neurons	AMAb91027	Atlas Antibodies	BX017	RX017-Atto550	1:50
NOP56 ribonucleoprotein	NOP56	Nucleoli	AMAb91013	Atlas Antibodies	BX029	RX029-Atto550	1:50
Neural proliferation, differentiation and control 1	NPDC1	Alpha cells	HPA008189	HPA	BX045	RX045-Cy5	1:100
Retinol binding protein 4	RBP4	Beta cells	ab226137	Abcam	BX031	RX031-Cy7	1:50
Somatostatin	SST	Delta cells	NBP2-37447	Novus Biologicals	BX020	RX020-Atto550	1:150
Tu translation elongation factor, mitochondrial	TUFM	Mitochondria	AMAb90966	Atlas Antibodies	BX021	RX021-Cy5	1:50

CODEX Antibody panel for multiplex tissue imaging of isolated pancreatic islets							
Target protein	**Target gene**	**Marker**	**Antibody Cat#**	**Manufacturer**	**Barcode**	**Reporter**	**Dilution**
Amylase, alpha 2A (pancreatic)	AMY2A	Pancreatic amylase	PA5-50358	Thermo Fisher	BX010	RX010-Cy7	1:100
Chromogranin A	CHGA	Neuroendocrine marker	NBP2-34674	Novus Biologicals	BX006	RX006-Cy5	1:100
Insulin	C-peptide	Beta cells	MA1-19159	Thermo Fisher	BX047	RX047-Atto550	1:50
Catenin beta 1	CTNNB1	Cell junctions	AMAb91209	Atlas Antibodies	BX033	RX033-Cy5	1:50
E-cadherin	CDH1	Cell adhesion	PN 4250021	Akoya Biosciences	BX014	RX014-Atto550	1:100

Ezrin	EZR	Plasma membrane	AMAb90976	Atlas Antibodies	BX036	RX036-Cy5	1:100
Shisa like 2B	FAM159B	Beta cells	HPA011778	HPA	BX054	RX054-Cy5	1:25
Glucagon	GCG	Alpha cells	MAB12491	R&D Systems	BX032	RX032-Atto550	1:100
Golgi reassembly stacking protein 2	GORASP2	Golgi apparatus	AMAb91016	Atlas Antibodies	BX027	RX027-Cy5	1:50
Grainyhead like transcription factor 2	GRHL2	Mesenchyme	# MA5-31388	Thermo Fisher	BX024	RX024-Cy5	1:50
Heat shock protein 90 beta family member 1	HSP90B1	ER	AMAb91019	Atlas Antibodies	BX030	RX030-Cy5	1:50
Islet amyloid polypeptide	IAPP	Beta cells	HPA053194	HPA	BX005	RX005-Atto550	1:100
Interleukin enhancer binding factor 3	ILF3	Beta cells	HPA001897	HPA	BX041	RX041-Atto550	1:100
Keratin 19	KRT19	Ductal cells	ab7754	Abcam	BX035	RX035-Atto550	1:100
Lamin B1	LMNB1	Nuclear membrane	AMAb91251	Atlas Antibodies	BX026	RX026-Atto550	1:50
MAF bZIP transcription factor A	MafA	Beta cells	ab264418	Abcam	BX042	RX042-Cy5	1:25
Neurofilament medium	NEFM	Neurons	AMAb91027	Atlas Antibodies	BX017	RX017-Atto550	1:50
NOP56 ribonucleoprotein	NOP56	Nucleoli	AMAb91013	Atlas Antibodies	BX029	RX029-Atto550	1:50
Neural proliferation, differentiation and control 1	NPDC1	Alpha cells	HPA008189	HPA	BX045	RX045-Cy5	1:100
Retinol binding protein 4	RBP4	Beta cells	ab226137	Abcam	BX031	RX031-Cy7	1:50
Somatostatin	SST	Delta cells	NBP2-37447	Novus Biologicals	BX020	RX020-Atto550	1:150
Tu translation elongation factor, mitochondrial	TUFM	Mitochondria	AMAb90966	Atlas Antibodies	BX021	RX021-Cy5	1:50

Appendix 5: The tables below present the reporter cycle arrangement and exposure times for each individual marker, and their respective fluorophore, used in the multiplex tissue imaging of the pancreas tissue section and isolated islets.

Reporter cycle arrangement for multiplex imaging of isolated pancreatic islets									
Well	**Cycle**	**DAPI Marker**	**DAPI Exposure** (ms)	**ATTO-550**	**Exposure time (ms)**	**Cy5**	**Exposure time (ms)**	**AF-750**	**Exposure time (ms)**
B2	1	DAPI1	50	Blank	750	Blank	750	Blank	750
B3	2	DAPI2	50	Blank	750	Blank	750	Blank	750
B4	3	DAPI3	50	ILF3	400	GORASP2	600	AMY2A	750
B5	4	DAPI4	50	C-pep	100	CTNNB1	600	Empty	10
B6	5	DAPI5	50	NOP56	500	FAM159B	750	Empty	10
B7	6	DAPI6	50	SST	50	EZR	400	Empty	10
B8	7	DAPI7	50	E-cadherin	500	MAFA	750	Empty	10
B9	8	DAPI8	50	IAPP	200	ACTB	500	Empty	10
B10	9	DAPI9	50	KRT19	300	HSP90B1	250	RBP4	750
B11	10	DAPI10	50	NEFM	600	CHGA	300	Empty	10
C2	11	DAPI11	50	GCG	50	NPDC1	750	Empty	10
C3	12	DAPI12	50	LMNB1	500	TUFM	750	Empty	10
C4	13	DAPI13	50	Blank	750	Blank	750	Blank	750
C5	14	DAPI14	50	Blank	750	Blank	750	Blank	750

Reporter cycle arrangement for multiplex imaging of isolated pancreatic islets									
Well	**Cycle**	**DAPI Marker**	**DAPI Exposure (ms)**	**ATTO-550**	**Exposure time (ms)**	**Cy5**	**Exposure time (ms)**	**AF-750**	**Exposure time (ms)**
B2	1	DAPI1	100	Blank	750	Blank	750	Blank	750
B3	2	DAPI2	100	ILF3	400	GORASP2	600	AMY2A	750
B4	3	DAPI3	100	C-pep	75	CTNNB1	600	Empty	10
B5	4	DAPI4	100	NOP56	500	FAM159B	750	Empty	10
B6	5	DAPI5	100	SST	50	EZR	400	Empty	10
B7	6	DAPI6	100	E-cadherin	500	MAFA	750	Empty	10
B8	7	DAPI7	100	IAPP	200	GRHL2	750	Empty	10
B9	8	DAPI8	100	KRT19	300	HSP90B1	250	RBP4	750
B10	9	DAPI9	100	NEFM	600	CHGA	300	Empty	10
B11	10	DAPI10	100	GCG	50	NPDC1	750	Empty	10
C2	11	DAPI11	100	LMNB1	500	TUFM	750	Empty	10
C3	12	DAPI12	100	Blank	750	Blank	750	Blank	750

Appendix 6: Examples of the cell segmentation predicted by the CODEX® Processor in the isolated pancreatic islets and pancreas tissue section, respectively. Two images are presented for each sample, one where no segmentation masks are present and only the nuclei are visualised in blue (Hoechst) and one where the segmentation masks are overlayed on the nuclei staining.